COVER PAGE

TITLE OF GRANT: "Ultra-high energy density relativistic plasmas from nanostructures: scaling to ultra-high intensities",

GRANT No. DE -SC0014610

FINAL REPORT

PERIOD OF PERFORMANCE: 8/15/2015- 8-14/2020

PI: Prof. Jorge Rocca
Department of Electrical & Computer Engineering
Colorado State University
Fort Collins, CO 80523
Phone: 970.491.8371
Email: Jorge.rocca@colostate.edu

DOE contact information: Dr. Kramer Akli, Fusion Energy Sciences
Email: Kramer.akli@science.doe.gov

FINAL REPORT DOE PLASMA
GRANT No. DE -SC0014610

Project abstract/summary

This project investigated the ultra-high energy density (UHED) regime of matter found in the center of stars, using a compact PW-class laser. These extreme conditions are typically only obtained in the laboratory in the central hot-spot of spherically imploded capsules in inertial confinement fusion experiments driven by the world's largest lasers. We have shown that near-solid density arrays of aligned nanostructures can be volumetrically heated to multi-keV temperatures by irradiation at relativistic intensity with ultrafast laser pulses of modest energy, opening a path for the generation of UHED plasmas with compact lasers. This new UHED plasma generation approach promises to create an environment with extreme energy densities and degrees of ionization, record conversion of optical laser light into ultrafast x-ray pulses, gigantic magnetic fields and pressures, and directed beams of high energy particles .

In this project we achieved record degree of ionization in volumetric heating solid density and near-solid density plasmas. Gold plasmas which spectra is characterized by L shell transition emission from ions with charge up to the Ne-like state, $Au+^{72}$ were generated using ultrafast laser pulses of less than 10 J of energy from a compact laser focused to an intensity of ~ $3x10^{21}$ Wcm^{-2}. **(R. Hollinger et al. *Nature Photonics, 14, 607, (2020)).*** We also conducted measurements to determine the heat penetration depth in Ni nanowire arrays as compared to Ni foil targets by monitoring the line emission of a Co buried tracer underneath a variable amount of Ni. The measurements revealed that the nanowire plasmas are roughly six times larger in depth than the solid density target plasmas. ***(C. Bargsten et al. Science Advances, 3 , e1601558 (2017)).*** A result of this increased plasma in nanowire arrays is a greatly increased conversion of optical laser light into > 1 KeV x-rays, ***(R. Hollinger et al. Optica, 4, 1344, (2017)),*** a record conversion efficiency of 20 %.

Critical to the realization of the proposed experiments was the generation of ultrafast laser pulses with ultra-high contrast that can deposit the energy deep into the nanowire arrays before the nanowires explode to create a continuous plasma. Supporting the proposed experiments was the recent demonstration at Colorado State University of a Petawatt-class laser that emits 30 fs pulses at high repetition rates. The experiments combined this unique laser tool with a variety of tailored nanowire arrays fabricated in house and with an extensive suite of diagnostics. The experiments were accompanied by 3-dimensional particle-in-cell simulations and detailed atomic physics simulations with transient kinetics and radiation transport. The proposed research allowed us to continue training Ph.D students and post-docs with broad experience in HEDP Science.

Journal Publications (2017-2020)

1. R. Hollinger, S. Wang, Y. Wang, A. Moreau, M.G. Capeluto, H. Song, A. Rockwood, E. Bayarsaikhan, V. Kaymak, A. Pukhov, V.N. Shlyaptsev and J.J. Rocca, "Extreme ionization of heavy atoms in solid density plasmas by relativistic second harmonic laser pulses"; Nature Photonics, **14**, 607, (2020)
2. [1] C. Bargsten, R. Hollinger, M. Gabriela Capeluto, V. Kaymak, A. Pukhov, S. Wang, A. Rockwood, Y. Wang, D. Keiss, R. Tommasini, R. London, J. Park, , V. N. Shlyaptsev, J.J.Rocca., "Energy penetration into arrays of aligned nanowires irradiated with relativistic intensities: scaling to terabar pressures", Science Advances, **3** , e1601558 (2017).
3. (3] R. Hollinger, B. Bargsten, V.N. Slyaptsev, V. Kaymak, A. Pukhov**,** M.G.Capeluto**,** S.Wang, A. Rockwood**,** Y. Wang, A. Towsend**,** A. Prieto, J.J. Rocca "Efficient picosecond X-ray pulses from plasma in the radiation dominated regime", Optica, **4**, 1344, (2017).
4. [5] Y. Wang, S. Wang, A. Rockwood, R. Hollinger, B. Luther, A. Curtis, C. Calvi, C.S. Menoni, and J.J. Rocca, " 0.85 PW laser operating at 3.3 Hz repetition rate and high contrast ultra high intensity 400 nm beamline", Optics Letters, 42, 3828, (2017).
5. J. J. Rocca, V. Shlyaptsev, R. Hollinger, C. Bargsten, A. Pukhov, V. Kaymak, R. Tommasini, R. London, J. Park, and M.G. Capeluto, "Compact Ultra-Intense Lasers and Nanostructures Open a Path to Extreme Pressures," Laser Focus World,. **53**, 21-26, (2017).

Conference Papers (2017-2020)

1. R. Hollinger, S. Wang, H. Song, Y. Wang, A. Moreau, M. Capeluto, V. Shlyaptsev, J.J. Rocca, A. Pukhov, J. Clark, and R. Shepherd, "Time Resolved Ni K Shell Spectroscopy of Nanowire Arrays Irradiated at Highly Relativistic Intensities" in 62nd *Annual Meeting of the APS Division of Plasma Physics*, virtual: APS BO04.00010 (2020).
2. J. J. Rocca, R. Hollinger, S. Wang, A. Curtis, C. Calvi, M. G. Capeluto, A. Moreau, Y. Wang, A. Rockwood, H. Song, V. N. Shlyaptsev, V. Kaymak, and A. Pukhov, "Highly relativistic ultrashort pulse laser interactions with ordered nanowire arrays: x-ray and neutron generation," in *International Conference on High Energy Density (ICHED),* (Oxford, United Kingdom, 2019). *Invited paper*
3. J. J. Rocca, R. Hollinger, V. N. Shlyaptsev, A. Curtis, C. Calvi, A. Moureau, M. G. Capeluto, V. Kaymak, A. Pukhov, Y. Wang, W. S, H. Song, and A. Rockwood, "Relativistic nanophotonics: creating extreme plasma conditions from nanostructures with ultrafast lasers," in *EPS Conference on Plasma Physics,* (Milan, Italy, 2019). *Invited paper*
4. R. Hollinger, A. Moreau, S. Wang, A. Rockwood, Y. Wang, M.G. Capeluto, V. Kaymak, A. Pukhov, V.N. Shlyaptsev, and J.J.Rocca; "Energy deposition of highly relativistic laser pulses into solid and near solid density high Z plasmas"; Bulletin of the American Physical Society Vol. 64, 11, paper YO4.0003, 61th Annual Meeting of the APS Division of Plasma Physics, Fort Lauderdale, Fl. October 20-25 (2019)
5. J. J. Rocca, "High power, high repetition rate lasers and applications to ultra-intense science," in *Quantum and Radiological Science and Technology (QST) International Symposium*, (Nara, Japan, 2018). *Invited paper*
6. J. J. Rocca, "Relativistic nanophotonics: creating extreme plasma conditions from nanostructures with ultrafast lasers," in *Annual High Energy Density Science Association Symposium at* APS Division of Plama Physics Annual Meeting. Portland, Oregon, (2018), *Invited paper*

7. J. J. Rocca, “Highly relativistic ultrashort pulse laser interaction with nanostructures: X-ray and neutron generation”, in *International Committee on Ultrahigh Intensity Lasers*.: Lindau, Germany. September (2018)
8. Y. Wang, S. J. Wang, A. Rockwood, B. M. Luther, R. Hollinge, A. Curtis, C. Calvi, C. S. Menoni, and J. J. Rocca, "High repetition rate petawatt laser and high-contrast ultra-high intensity second harmonic beamline," in *2018 IEEE Photonics Conference*, Reston, Virginia, 2018.
9. J. J. Rocca, R. Hollinger, V. N. Shlyaptsev, M. G. Capeluto, A. Curtis, C. Calvi, S. Kasdorf, V. Kaymak, A. Pukhov, Y. Wang, S. Wang, and A. Rockwood, "Extreme conditions from ultra-intense femtosecond laser pulses interacting with aligned nanostructures," in *OSA Frontiers in Optics/Laser Science Conference (FiO/LS),* (Washington, DC, 2018). Invited paper.
10. S. Wang, Y. Wang, A. Rockwood, B. M. Luther, R. Hollinge, A. Curtis, C. Calvi, C. S. Menoni, and J. J. Rocca, "PW-class Laser Operation at 3.3 Hz and High Contrast Ultra-intense λ=400 nm Beamline," in *Conference on Lasers and Electro-Optics*, OSA Technical Digest (online) (Optical Society of America, 2018), STu3M.1.
11. J. J. Rocca, R. Hollinger, V.N. Shlyaptsev, M.G. Capeluto, V. Kaymak, A. Pukhov, A. Curtis, C. Calvi, C. Bargsten, Y. Wang, S. Wang, and A. Rockwood, "Relativistic nanophotonics: heating matter to extreme conditions with compact lasers" in *Winter Colloquium on the Physics of Quantum Electronics*, Snowbird, Utah: Journal of Modern Optics Abstract d/718 (2018). Invited Paper.
12. R.C. Hollinger, A.F. Moreau, M.G. Capeluto, Y. Wang, S. Wang, A.P. Rockwood, A.H. Curtis, C.N. Calvi, V. Kaymak, A. Pukhov, V.N. Shlyaptsev, and **J. J. Rocca**, "Au L shell emission from nanowire arrays irradiated at highly relativistic intensities" in *Annual Meeting of the APS Division of Plasma Physics*, Portland, Oregon: APS JO8.00013 (2018).
13. A.F. Moreau, R.C. Hollinger, M.G. Capeluto, S. Wang, Y. Wang, A.P. Rockwood, V. Kaymak, A. Pukhov, A.H. Curtis, C.N. Calvi, V.N. Shlyaptsev, and **J. J. Rocca**, "Dynamics of energy deposition of highly relativistic laser pulses in aligned nanowire arrays" in *Annual Meeting of the APS Division of Plasma Physics*, Portland, Oregon: APS JO8.00012 (2018).
14. R. Hollinger, Y. Wang, S. Wang, A. Rockwood, J. Glasby, V. Shlyaptsev, J. J. Rocca, M.G. Capeluto, V. Kaymak, and A. Pukhov, "Ultra high energy density plasmas generated by highly relativistic laser nanowire interactions" in *Annual Meeting of the APS Four Corners Section*, Fort Collins, Colorado: APS L6.00001 (2017).
15. R.C. Hollinger, Y. Wong, S. Wong, A. Rockwood, J. Glasby, V. Shlyaptsev, J. J. Rocca, M.G. Capeluto, V. Kaymak, and A. Pukhov, "Nanostructure array plasmas generated by femtosecond pulses at highly relativistic intensities" in *Annual Meeting of the APS Division of Plasma Physics*, Milwaukee, Wisconsin: APS TO8.00008 (2017).

What was accomplished under these goals?

The main results obtained are briefly summarized below, and in full extent in the published journal papers, three of which are attached.

We have achieved volumetric heating of solid density and near-solid density gold plasmas characterized by L shell transition array spectra with emission from ions with charge up to the Ne-like state, $Au+^{72}$ using ultrafast laser pulses of less than 10 J of energy from a compact laser focused to an intensity of $3x10^{21}$ Wcm^{-2}. **(R. Hollinger et al. *Nature Photonics, 14, 607, (2020)).*** We also conducted experiments using Ni nanowire arrays and Ni foils targets that led to the observation of H-like emission exceeding half the intensity of the He-like transitions. The results show that at these

intensities (a_o~19) it is possible to volumetrically heat solid targets to depths of >1um, and aligned nanowire plasmas with 17 % solid density to > 6um in depth .The study shows that while solid foil targets reach slightly higher degree of ionization at these highly relativistic irradiation intensities due to an increased collision excitation rate, the much larger plasma volume from irradiating arrays of nanowires results in one order of magnitude higher conversion efficiency into > 1 KeV x-rays. These conditions are found to exist in a significant volume-- up to a micron in depth in solid density targets and up to 6um in depth in ordered nanowire arrays.

A distinguishing feature of nanowire arrays as compared with solid targets is extended volumetric hearing. During this project we conducted measurements to determine the heat penetration depth in Ni nanowire arrays as compared to Ni foils by monitoring the line emission of a Co buried tracer underneath a variable amount of Ni ***(C. Bargsten et al. Science Advances, 3 , e1601558 (2017))*** The Ly-α and He-α spectral emission from the Co tracer was monitored while varying the thickness of the nickel layer. These materials were chosen since they differ by a Z of one. The He-like Co line intensity was observed to decrease with respect to the He-like and H-like Ni lines as the Ni top layer increases in thickness. When the Co is underneath 1um of Ni, the Co He lines are still visible indicating a penetration depth of slightly greater than 1um in solid density Ni. This increase in the heat penetration depth is, at least in part, due the modification of the critical electron density from relativistic transparency. While the critical electron density for λ=400nm is 6.87x10^{21} cm^{-3} , at a_o=20 corresponding to this experiments the relativistically corrected value exceeds 1x10^{23} cm^{-3} , allowing for significantly higher penetration depth of the laser energy into the solid density and nanowire targets. Measurements were also conducted for nanowire arrays consisting of 55nm diameter dual composition (Ni-Co) wires at 12% of solid density with 6um of Ni on top of 3um of Co for comparison. The He-like Co lines are visible still under 6um of Ni at an intensity of 4x$10^{21}$$Wcm^{-2}$ revealing that the nanowire plasmas are roughly six times larger in depth than the solid density target plasmas.

Another result obtained in this investigation of nanowire arrays plasmas is the greatly increased conversion of optical laser light into > 1 KeV x-rays. ***(R. Hollinger et al. Optica, 4, 1344, (2017))***. The efficient conversion of optical laser light into bright ultrafast x-ray pulses in plasmas is of high interest for dense plasma physics studies, material science, and other fields. However, the rapid hydrodynamic expansion that cools hot plasmas typically limits the conversion efficiency (CE) of conversional plasmas to 1% or less. In this project we demonstrated a more than an order of magnitude increase in x-ray CE by tailoring near solid density plasmas to achieve a large radiative-to-hydrodynamic energy loss rate ratio, leading into a radiation loss dominated plasma regime. A record CE into hν > 1keV photons of ~ 20% in 4π sr was measured volumetrically heating arrays of large aspect ratio Au nanowires to keV temperatures with ultrahigh contrast femtosecond laser pulses of relativistic intensity.

The lateral extent of these multi-keV radiation plasma sources was measured by monitoring the x-ray source size with point projection radiography on a tungsten carbide (WC) sphere. The sphere suffers no parallax and is sufficiently high Z to block

x-rays from propagating through it. By observing the width of the penumbra, it is possible to calculate the x-ray source size. Radiographs of a 500um WC sphere setup placed at approximately 6cm from the plasma were obtained for both a solid density target and for a nanowire target. A filter consisting of 13um of Be and 50um of Al was placed in front of the CCD to filter out photons <6keV. The lineout of the edge of the sphere is plotted for both targets and deconvolved with the magnification of the imaging system to show the source size. The source size is found to be 6um for the solid density target while it is 10um for the nanowire array target, a ratio of 2.7 for surface area. This can be explained by the fact that the diffusive heat wave propagates laterally with a velocity proportional to $1/\sqrt{n_e}$. For the nanowire plasma measured at 15% of solid density, the heat wave propagates at a velocity 2.5 faster than a solid density plasma at the same temperature. The potential of these bright ultrafast table-top point x-ray sources in imaging applications was illustrated with single shot flash radiographs obtained with very low laser pulse energy. These results will enable the deployment of brighter laser-driven x-ray sources at both compact and large laser facilities.

In summary, experiments were conducted irradiating arrays of ordered nanowires of solid Au and Ni targets and solid foils of the same materials. The results obtained demonstrate that highly relativistic femtosecond laser pulses of only 10 J energy can volumetrically deposit energy deep into solid density and near solid density plasmas characterized by record high degree of ionization (e.g. N-like Au , Au^{+72}). The study shows that while solid foil targets reach slightly higher degree of ionization at these highly relativistic irradiation intensities, the heat penetration depth and therefore the volume of plasma heated is several times larger in the nanowire targets, resulting in more efficient conversion into x-rays. A record 20% CE into $h\nu$ > 1keV photons in 4π sr was measured volumetrically irradiating arrays of large aspect ratio Au nanowires with ultrahigh contrast femtosecond laser pulses of relativistic intensity .

nature photonics

LETTERS

https://doi.org/10.1038/s41566-020-0666-1

Extreme ionization of heavy atoms in solid-density plasmas by relativistic second-harmonic laser pulses

R. Hollinger[1]✉, S. Wang[1], Y. Wang[1], A. Moreau[1], M. G. Capeluto[1,2], H. Song[1], A. Rockwood[3], E. Bayarsaikhan[3], V. Kaymak[4], A. Pukhov[4], V. N. Shlyaptsev[1] and J. J. Rocca[1,3]✉

Stripping heavy atoms in solid matter of most of their electrons requires the extreme conditions that exist in astrophysical plasmas, but are difficult to create in the laboratory[1-3]. Here we demonstrate solid-density gold plasmas with atoms stripped of up to 72 electrons (N-like Au^{72+}) over large target depths. This record ionization is achieved by irradiating solid foils and near-solid-density nanowire arrays with highly relativistic (3×10^{21} W cm^{-2}) second-harmonic femtosecond laser pulses of <10 J energy focused into a 1.6 μm spot. The short wavelength and high intensity enable the interaction to occur at a relativistic critical density[4,5] of 10^{23} cm^{-3}. Solid targets reach a higher average charge in 1- to 2-μm-thick layers, while the less dense nanowire plasmas are heated to much larger depths (>8 μm) by energetic electrons generated near the nanowire tips. Larger laser spots could result in solid Au plasmas ionized up to He-like.

Extending the accessible states of matter in the laboratory into extreme unexplored regimes can provide a new understanding of the behaviour of atoms in such environments, leading to the discovery of new phenomena and applications. The ability to generate data from solid-density plasmas with unprecedented degrees of ionization will provide much needed benchmarks to extend the capability of models to simulate ultrahigh energy density states of matter. For example, a comparison of high-resolution X-ray spectra with advanced atomic codes could lead to new insights into the behaviour of extremely charged atoms in intense micro-fields and also address new questions on the physics of these ions in solid-density environments. Au atoms at densities over 10 orders of magnitude below solid density have been ionized up to the Ne-like stage (Au^{69+}) by collisions with a high-energy electron beam while being trapped in a potential well, producing high-quality L-shell spectra over a broad range of high ion charges[6,7]. Achieving similar degrees of ionization in near-solid-density plasmas requires the deposition of ultrahigh energy densities, leading to extreme temperatures and high collisional ionization rates. High degrees of ionization have been achieved in dense plasmas driven by laser pulse energies of several hundred joules to kilojoules. Experiments conducted at the OMEGA laser using 9 kJ pulses of nanosecond duration to heat a reduced-scale 'hot' hohlraum revealed strong L-shell Au emission with an average charge state of Ti-like Au^{57+} and an inferred temperature of 6.5 keV at an electron density of 10^{21} cm^{-3} (ref. [3]). For mid-atomic-number (Z) elements such as Ni, measurements performed at intensities up to 5×10^{20} W cm^{-2} with 400 J pulses of 0.8 ps duration revealed emission from the He-α and Ly-α transitions and a surface temperature of 5 keV decreasing to 600 eV at a depth of 1.3 μm (ref. [8]). Temperatures of 600 eV in Al foils buried under 10 μm of CH were measured by K-shell emission spectroscopy when irradiated by 100 J pulses of 0.5 ps duration[9]. Buried Cu tracers irradiated at an intensity of $>10^{20}$ W cm^{-2} (140 J, 1.053 μm, 500 fs duration) at the Titan short pulse laser exhibited a large amount of He-like emission with an estimated surface temperature of 2,100 eV (ref. [10]). Experiments irradiating 12% solid-density Au nanowire arrays at an intensity of 5×10^{18} W cm^{-3} generated plasmas ionized to charge states up to Au^{52+} (ref. [11]).

Here we demonstrate the generation of solid- and near-solid-density Au plasmas characterized by L-shell line emission from atoms ionized up to the N-like state Au^{72+}, an unprecedented degree of ionization for dense laboratory plasmas. Moreover, this was achieved using femtosecond laser pulses of less than 10 J energy, which can be generated at high repetition rates. The experimental results were obtained using high-contrast second-harmonic $\lambda=400$ nm laser pulses focused to a highly relativistic intensity of $\sim3\times10^{21}$ W cm^{-2}, corresponding to a normalized vector potential of the laser field of $a_0=18.6$. At this intensity, relativistic effects increase the critical electron density (n_{crit}) by a factor of $\gamma\approx13$ to $n_{crit\ rel}\approx10^{23}$ cm^{-3} ($n_{crit\ rel}=\gamma n_{crit}$; relativistic factor $\gamma=\sqrt{1+\frac{a_0^2}{2}}$). This increase in the critical density makes it is possible to volumetrically deposit energy generating highly ionized atoms deeper into overdense media. We compare results from solid slab targets to those obtained when irradiating nanowire arrays, which previous studies at lower intensities have shown to result in enhanced X-ray emission[12–16]. We show that, at these highly relativistic intensities, it is possible to volumetrically heat solid-density plasmas to depths of >1 μm (with an estimated energy deposition density of up to 10 GJ cm^{-3}) and aligned nanowire arrays with 15% solid density to depths >8 μm. For nanowires, the average volumetric energy density approaches 100 GJ cm^{-3}, an ultrahigh energy density regime that is virtually unexplored in laboratory plasmas. Three-dimensional (3D) particle-in-cell (PIC) simulations show that the mechanism of energy deposition deep into the nanowire target differs from those at lower irradiation intensity and is dominated by energetic electrons accelerated near the target surface.

The experiments were conducted by irradiating gold foils and nanowire arrays with a frequency-doubled Ti:sapphire laser[17] delivering ultrahigh-contrast ($>10^{12}$), $\lambda=400$ nm pulses of 45 fs duration

[1]Electrical and Computer Engineering Department, Colorado State University, Fort Collins, CO, USA. [2]Departamento de Física, Universidad de Buenos Aires – IFIBA, Ciudad Universitaria, Buenos Aires, Argentina. [3]Physics Department, Colorado State University, Fort Collins, CO, USA. [4]Institut für Theoretische Physik, Heinrich-Heine-Universität Düsseldorf, Düsseldorf, Germany. ✉e-mail: reed.hollinger@colostate.edu; jorge.rocca@colostate.edu

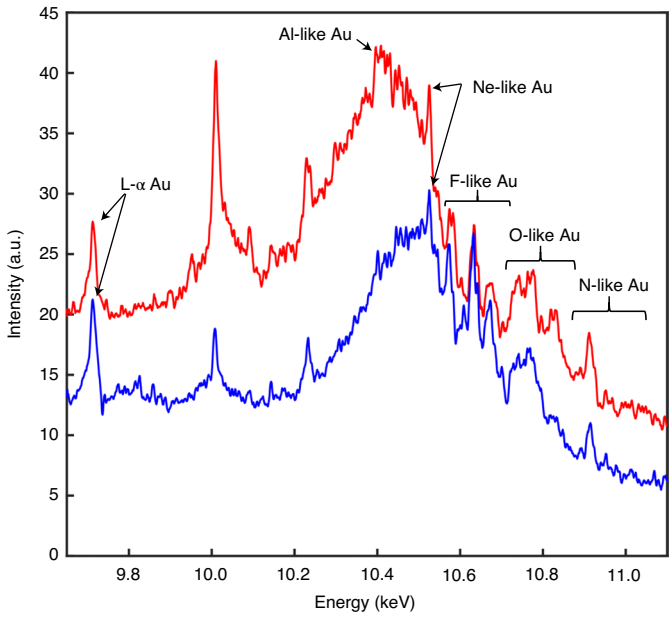

Fig. 1 | L-shell emission from solid-density Au foils and Au nanowire arrays. L-shell emission from solid-density Au foils (blue curve) and 100-nm-diameter Au nanowire arrays at 15% of solid density (red curve) irradiated at 3×10^{21} W cm^{-2}. Line emission from charge states including Ne-like Au^{69+}, F-like Au^{70+}, O-like Au^{71+} and N-like Au^{72+} is observed for both targets. The line feature near 10.92 keV has contributions of N-like Au^{72+} and O-like Au^{71+}. The charge state distribution is centred around Al-like Au^{66+} for the nanowire plasma and Ne-like Au^{69+} for the solid foil plasma.

on target. The use of second harmonics suppresses laser pre-pulses and leads to higher critical densities and, consequently, increased collisional rates. The L-shell emission of Au was monitored using a moderate-resolution ($E/\Delta E \approx 1{,}000$) Von Hamos mica crystal spectrometer. Figure 1 shows spectra corresponding to both a Au foil target and a 100-nm-diameter Au nanowire array with 15% of solid density. Both targets display emission from the Ne-like Au transition, at 10,525 eV as well as lines corresponding to higher ionization stages up to N-like Au^{72+}. The average charge state is measured to be Al-like Au^{66+} for nanowires and at Ne-like Au^{69+} for solid targets, which is substantially higher than reported in previous work. Simulated spectra computed with the hydrodynamic/atomic physics code RADEX using initial conditions from the PIC simulations agree with the experiment in showing line emission from ions up to N-like Au^{72+} (Extended Data Fig. 1).

The energy penetration depth at this intensity was measured by monitoring the He-α line emission (Fig. 2a–d) from a buried Ni tracer under a variable amount of solid Au (inset, Fig. 2e). Figure 2c shows that He-like Ni line emission is still visible when the Ni tracer is under 1 μm of solid Au. A summary of the He-like Ni emission intensity versus buried depth is plotted in Fig. 2e. The much larger laser heat penetration in the nanowire arrays was demonstrated using an array of dual-composition 100-nm-diameter wires with 15% of solid density consisting of an 8-μm Au nanowire segment on top of a 3 μm Ni segment. The He-like Ni lines are still visible under 8 μm of Au, revealing that the nanowire plasmas are significantly larger in volume than the solid-density target plasmas. This was simultaneously measured to contribute to an increase in the $h\nu > 1$ keV X-ray emission with respect to the foil targets (Extended Data Fig. 2) due to the increase in hydrodynamic cooling time compared with the plasma radiative lifetime.

PIC simulations show that, at these highly relativistic intensities, the mechanism by which energy is deposited deep into the dense array of small-diameter nanowires differs from that at lower intensities, where laser light penetrates deep into the interwire gaps[11]. Figure 3 shows the results for a 15% solid-density array of 100-nm-diameter Au nanowires. The electron density in units of $n_{crit} = 6.9\times10^{21}$ cm^{-3} (Fig. 3a–c), the electric field propagation (Fig. 3d–f) and the ionization state (Fig. 3g–i) are shown for three different times: −30 fs, 0 fs and +1,000 fs with respect to the peak of the laser pulse. Initially, the electric field of the laser propagates in the interwire gap down the length of the wire, accelerating electrons towards the substrate (Fig. 3a). As the laser intensity increases, a large electric field at the nanowire tips drives optical field ionization up to Ne-like Au^{69+} and accelerates the electrons towards the substrate (Fig. 3h). The nanowires begin to pinch due to a quasi-static self-generated magnetic field generated by the return electron current[18] through the wires, and the peak electron density within the wires exceeds $1{,}000 n_{crit}$ (Fig. 3e). The wire tips are rapidly heated by electron collisions and explode before the peak of the laser pulse arrives (Fig. 3b), filling the gaps with an overdense plasma greater than 15 times the critical density, which is higher than even the relativistic critical density. After this time, the laser can no longer propagate into the nanowire array. However, the laser heats up the thin surface layer, depositing a majority of the energy into a thin slab of overdense plasma, which reaches a peak electron energy density of >1,000 GJ cm^{-3} (Extended Data Fig. 3). Energetic electrons emanating from this layer propagate down the length of the wires, depositing their energy into the array and ionizing atoms up to the N-like stage in the entire volume. The average degree of ionization, Al-like Au^{66+}, is lower than in the solid-density plasmas, but the plasma depth is nearly an order of magnitude higher, in agreement with the experimental observations.

In contrast to the nanowire target, the solid-density target volume is overdense for the entire duration of the laser pulse. The laser energy is absorbed mainly by collisionless processes[19] with electrons and ions in a layer that is much thinner than the nanowire-array skin depth, causing less efficient energy absorption. A large population of energetic electrons generated within the skin depth transport the energy deep into the solid-density target, where current filaments give rise to Weibel instabilities[20] (Extended Data Fig. 4). In the 3D PIC simulation for solid-density Au slab targets presented in Fig. 4, the ionization of atoms to high charge states at +500 fs after the peak of the laser pulse is computed to propagate ~2 μm into the target, a value similar to that inferred from spectral measurements. This is in contrast to solid-density foils irradiated at much lower intensity, where only a thin layer is heated[21]. This larger depth of heated solid-density plasma increases the hydrodynamic expansion time, resulting in a new volumetrically heated solid-density plasma regime with an extreme degree of ionization. At non-relativistic intensities, the second or third harmonic of optical lasers is usually used to increase the absorption in flat targets at normal incidence. By comparison, the combination of the second harmonic with the relativistically modified critical density increases n_{crit} to ~10^{23} cm^{-3}, corresponding to that of the 10th harmonic of a 1 μm laser, effectively increasing absorption. Although the overall absorption of flat solid targets is still smaller than for nanowires, its increase, along with the increase in collisional rate, allows solid targets to reach and even surpass the average Z in nanowires. Instead, it has been shown previously that, at lower intensities, solid targets generate much lower temperatures and lower ionization degrees than nanowires. The study of the plasma dynamics predicted by the PIC simulation will require ultrafast probes. For example, the intense femtosecond pulses from X-ray free-electron lasers will allow for Thomson scattering measurements of the plasma parameters once petawatt-class lasers capable of generating the plasmas reported here are implemented at those facilities.

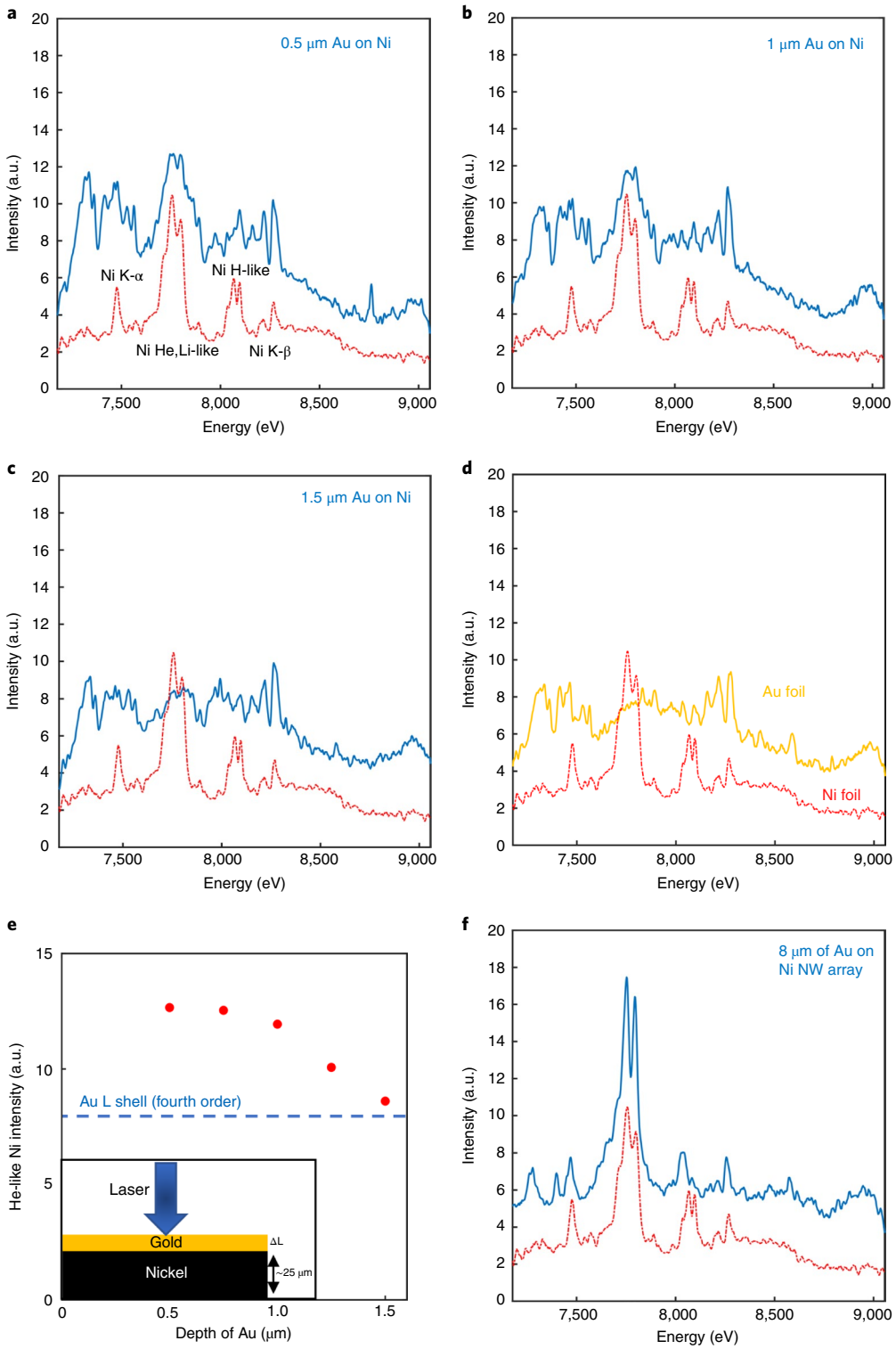

Fig. 2 | Energy penetration depth determined with buried layer spectroscopy. a–d, Single-shot spectra of Ni tracer (blue) buried under varying amounts of gold (0.5μm (**a**); 1μm (**b**) and 1.5μm (**c**)) compared with the spectra of a pure Au foil (**d**). Pure Ni foil reference spectra are plotted in red in each plot. **e**, Integrated He-like Ni intensity versus Au thickness. Inset: structure of the targets used in the tracer experiment. **f**, Spectra showing the much deeper heat penetration depth in the nanowire (NW) array, corresponding to segmented 100-nm-diameter Au nanowires that are 8μm in length with an average density corresponding to 15% solid on top of 3μm of Ni nanowires.

Simulations also predict that irradiation of solid targets with the same intensity over a larger spot using the upcoming new generation of multi-petawatt lasers will create solid-density plasmas with atoms ionized up to He-like Au (Extended Data Fig. 5) over even larger penetration depths. This will result from the reduced plasma expansion rate associated with the larger plasma volume maintaining an extremely hot plasma with a density close to the relativistic critical density, for a longer time. The minimum spot size

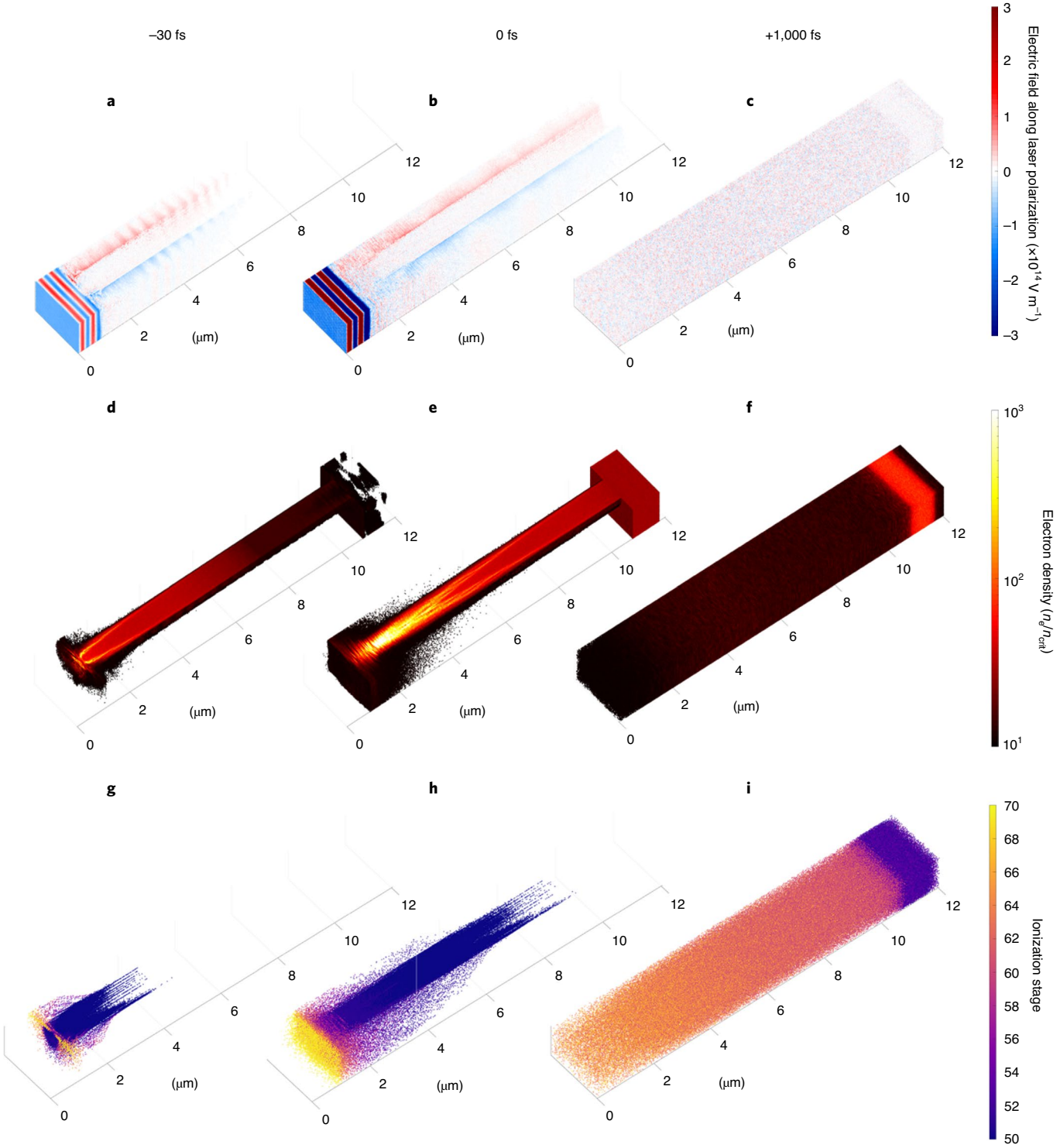

Fig. 3 | PIC simulation results for a 15% solid-density array of 100-nm-diameter Au nanowires. a–i, 3D PIC simulations for an array of 100-nm-diameter Au nanowires with an average density corresponding to 15% solid density showing the evolution of the driving electric field (**a**–**c**), electron density (**d**–**f**) and ionization state (**g**–**i**) at three different times: 30 fs preceding the peak of the laser pulse (**a**,**d**,**g**), at the peak of the laser pulse (**b**,**e**,**h**) and +1,000 fs afterwards (**c**,**f**,**i**). The electron density is plotted in units of n_{crit} (6.87×10^{21} cm^{-3} for $\lambda=400$ nm) and only for densities $>15n_{crit}$.

necessary to reach the He-like ionization state is estimated to be ~5 μm. These unprecedented degrees of ionization in solid-density and near-solid-density nanostructure plasmas will open the door to the study of the atomic physics of highly charged atoms in very high-density plasmas, including, for example, phenomena such as line broadening, line shifts and continuum lowering. These unique plasmas will also enable applications such as beams of highly charged particles and more efficient X-ray radiation sources.

Online content

Any methods, additional references, Nature Research reporting summaries, source data, extended data, supplementary information,

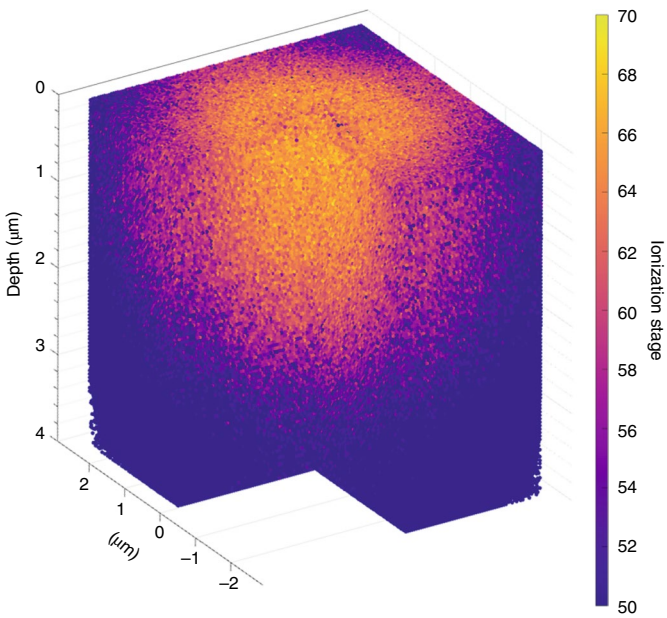

Fig. 4 | Three-dimensional PIC simulation showing the degree of ionization for a solid-density Au slab target. The target is irradiated at an intensity of 4×10^{21} W cm^{-2}, +500 fs following the peak of the laser pulse.

acknowledgements, peer review information; details of author contributions and competing interests; and statements of data and code availability are available at https://doi.org/10.1038/s41566-020-0666-1.

Received: 17 December 2019; Accepted: 18 June 2020;
Published online: 20 July 2020

References

1. Heeter, R. F. et al. Benchmark measurements of the ionization balance of non-local thermodynamic-equilibrium gold plasmas. *Phys. Rev. Lett.* **99**, 195001 (2007).
2. Foord, M. E. et al. Ionization processes and charge-state distribution in a highly ionized high-*Z* laser-produced plasma. *Phys. Rev. Lett.* **85**, 992–995 (2000).
3. May, M. J. et al. X-ray spectral measurements and collisional-radiative modeling of hot, gold plasmas at the omega laser. *High Energy Density Phys.* **4**, 78–87 (2008).
4. Kaw, P. & Dawson, J. Relativistic nonlinear propagation of laser beams in cold overdense plasmas. *Phys. Fluids* **13**, 472–481 (1970).
5. Palaniyappan, S. et al. Dynamics of relativistic transparency and optical shuttering in expanding overdense plasmas. *Nat. Phys.* **8**, 763–769 (2012).
6. Träbert, E. et al. L-shell spectroscopy of Au as a temperature diagnostic tool. *Rev. Sci. Instrum.* **79**, 10E313 (2008).
7. Brown, G. V. et al. Investigation of the $2p_{3/2}$–$3d_{5/2}$ line emission of Au^{53+}–Au^{69+} for diagnosing high energy density plasmas. *Phys. Rev. E* **77**, 066406 (2008).
8. Akli, K. U. et al. Laser heating of solid matter by light-pressure-driven shocks at ultrarelativistic intensities. *Phys. Rev. Lett.* **100**, 165002 (2008).
9. Hoarty, D. J. et al. Observations of the effect of ionization-potential depression in hot dense plasma. *Phys. Rev. Lett.* **110**, 265003 (2013).
10. Chen, S. N. et al. X-ray spectroscopy of buried layer foils irradiated at laser intensities in excess of 10^{20} W/cm^2. *Phys. Plasmas* **16**, 062701 (2009).
11. Purvis, M. A. et al. Relativistic plasma nanophotonics for ultrahigh energy density physics. *Nat. Photon* **7**, 796–800 (2013).
12. Kulcsar, G. et al. Intense picosecond X-ray pulses from laser plasmas by use of nanostructured 'Velvet' targets. *Phys. Rev. Lett.* **84**, 5149–5152 (2000).
13. Nishikawa, T. et al. Nanocylinder-array structure greatly increases the soft X-ray intensity generated from femtosecond-laser-produced plasma. *Appl. Phys. B* **73**, 185–188 (2001).
14. Ovchinnikov, A. V. et al. Characteristic X-rays generation under the action of femtosecond laser pulses on nano-structured targets. *Laser Part. Beams* **29**, 249–254 (2011).
15. Mondal, S. et al. Highly enhanced hard X-ray emission from oriented metal nanorod arrays excited by intense femtosecond laser pulses. *Phys. Rev. B* **83**, 035408 (2011).
16. Hollinger, R. et al. Efficient picosecond X-ray pulse generation from plasmas in the radiation dominated regime. *Optica* **4**, 1344–1349 (2017).
17. Wang, Y. et al. 0.85 PW laser operation at 3.3 Hz and second-harmonic beamline. *Opt. Lett.* **42**, 3828–3831 (2017).
18. Kaymak, V., Pukhov, A., Shlyaptsev, V. N. & Rocca, J. J. Nanoscale ultradense Z-pinch formation from laser-irradiated nanowire arrays. *Phys. Rev. Lett.* **117**, 035004 (2016).
19. Levy, M. C., Wilks, S. C., Tabak, M., Libby, S. B. & Baring, M. G. Petawatt laser absorption bounded. *Nat. Commun.* **5**, 4149 (2014).
20. Weibel, E. S. Spontaneously growing transverse waves in a plasma due to an anisotropic velocity distribution. *Phys. Rev. Lett.* **2**, 83–84 (1959).
21. Rosmej, O. N. et al. Generation of keV hot near-solid density plasma states at high contrast laser-matter interaction. *Phys. Plasmas* **25**, 083103 (2018).

Publisher's note Springer Nature remains neutral with regard to jurisdictional claims in published maps and institutional affiliations.

© The Author(s), under exclusive licence to Springer Nature Limited 2020

Methods

Experimental. The experiments were conducted using laser pulses from the petawatt-class ALEPH Ti:sapphire laser developed at Colorado State University. The pulses were compressed to 45 fs and were subsequently frequency-doubled using an 800-μm-thick type 1 second-harmonic-generation potassium diphosphate crystal. A contrast $>10^{12}$ is obtained after the second harmonic is separated from the fundamental using a series of five dichroic mirrors. A deformable mirror was used before the compressor to correct static aberrations in the wave front. The pulses were focused by an *f*/2, 45° off-axis parabola to achieve an intensity of up to 3×10^{21} W cm^{-2} on target. Single-shot X-ray spectroscopy was performed using a mica crystal ($2d=19.84$ Å) with a radius of curvature of 40 mm in a Von Hamos configuration in the third order. The spectrographs were recorded on a Fujifilm BAS MS image plate and read out immediately after every shot to avoid fading. The spectra are single shot. The experiment has good reproducibility (for example, see Extended Data Fig. 6 for three consecutive single-shot spectra obtained under the same irradiation conditions). Measurement of the energy penetration depth into the target was conducted by monitoring the ionized K shell of a buried Ni layer seen in the third order of a mica crystal. The L shell of Au is also present from the fourth order of the mica crystal, which has a significantly lower integrated reflectivity[22]. The L-shell spectra were calibrated using the well-resolved He-like and H-like transitions from the K shell of Ge at 10,274 eV and 10,569 eV (Extended Data Fig. 7). The X-ray yield was simultaneously measured using a filtered Si photodiode (AXUV100-G, International Radiation Detectors). A photodiode with a 13-μm-thick Be filter was placed 2.5 m from the plasma at 45° with respect to the target normal to monitor the $h\nu>1$ keV X-ray emission. Large surface areas of high-aspect-ratio, aligned nanowires were fabricated through electrodeposition of Ni and Au into anodic aluminium oxide wafers.

PIC simulations. Both the solid-density and nanowire-array plasmas were simulated with a relativistic 3D PIC code Virtual Laser Plasma Laboratory[23]. This code is the same as that used to perform nanowire plasma simulations in ref. [11], with atomic data added for high-*Z* elements. The spectra were simulated using the radiative/hydrodynamic code RADEX[24], with detailed atomic physics using data from the HULLAC code[25]. The PIC code standard algorithms were extended by packages for optical field ionization (OFI) and binary collisions, including electron impact ionization. OFI was treated as an under barrier tunnelling phenomenon in the static electric field[26,27], with only sequential field ionization considered. The probabilities for Coulomb collisions between all particles in one mesh cell were calculated by a binary collision package. PIC simulations utilized a 3D geometry and self-consistently included ionization physics. A linearly polarized plane wave with $\lambda=400$ nm and temporal Gaussian pulse profile with a duration of 45 fs full-width at half-maximum (FWHM) was used to simulate the laser pulse with the normalized vector potential $a_o = eA/(mc^2)=21$ for a laser intensity of 4×10^{21} W cm^{-2}. The laser impinged on the nanowire array and solid-density target at normal incidence. The PIC simulation space consisted of a cell volume encompassing the wire and interwire gaps, as well as space above the target to allow for expansion as it thermalized.

Data availability

The data that support the plots within this paper and other findings of this study are available from the corresponding authors upon reasonable request.

Code availability

The computer programs that support the findings of this study can be made available upon reasonable request to the corresponding authors.

References

22. Sánchez del Río, M., Faenov, A. Y., Pikuz, T. A., Souvorov, A. & Freund, A. K. Hard X-ray reflectivity of spherically bent mica crystals. *AIP Conf. Proc.* **521**, 287–2292 (2000).
23. Pukhov, A. & Meyer-ter-Vehn, J. Laser hole boring into overdense plasma and relativistic electron currents for fast ignition of ICF targets. *Phys. Rev. Lett.* **79**, 2686–2689 (1997).
24. Shlyaptsev, V. N., Rocca, J. J. G. & Osterheld, A. L. Dynamics of a capillary discharge X-ray laser. *Proc. SPIE* **2520**, 365–372 (1995).
25. Bar-Shalom, A., Klapisch, M. & Oreg, J. HULLAC, an integrated computer package for atomic processes in plasmas. *J. Quant. Spectrosc. Radiat. Transf.* **71**, 169–188 (2001).
26. Karmakar, A. & Pukhov, A. Collimated attosecond GeV electron bunches from ionization of high-*Z* material by radially polarized ultra-relativistic laser pulses. *Laser Part. Beams* **25**, 371–377 (2007).
27. Zhidkov, A. & Sasaki, A. Effect of field ionization on interaction of an intense subpicosecond laser pulse with foils. *Phys. Plasmas* **7**, 1341–1344 (2000).

Acknowledgements

The experiments were conducted using the Colorado State University ALEPH laser facility supported by LaserNet US (DE-SC0019076). The work was supported by Fusion Energy Sciences (FES), Office of Science, of the US Department of Energy (DOE) (grant no. DE-SC0014610). R.H. was supported by the US DOE FES Postdoctoral Research Program administered by the Oak Ridge Institute for Science and Education (ORISE) for the DOE. ORISE is managed by Oak Ridge Associated Universities (ORAU) under DOE contract number DE-SC0014664. All opinions expressed in this paper are the author's and do not necessarily reflect the policies and views of DOE, ORAU or ORISE. The simulations were conducted using the Colorado University/Colorado State University Summit High Performance Computer System, National Science Foundation (ACI-1532235). We acknowledge the assistance of T. Kaiser in running the PIC code.

Author contributions

The concept of the experiment was proposed by R.H. and J.J.R. and the experiment was designed by R.H., Y.W., S.W. and J.J.R. Modelling was performed by V.N.S., R.H., V.K. and A.P. The experiments were conducted by R.H., A.M., S.W., Y.W., H.S. and A.R. The targets were developed and manufactured by M.G.C., E.B. and R.H. All authors participated in the writing of the manuscript.

Competing interests

The authors declare no competing interests.

Additional information

Extended data is available for this paper at https://doi.org/10.1038/s41566-020-0666-1.

Correspondence and requests for materials should be addressed to R.H. or J.J.R.

Reprints and permissions information is available at www.nature.com/reprints.

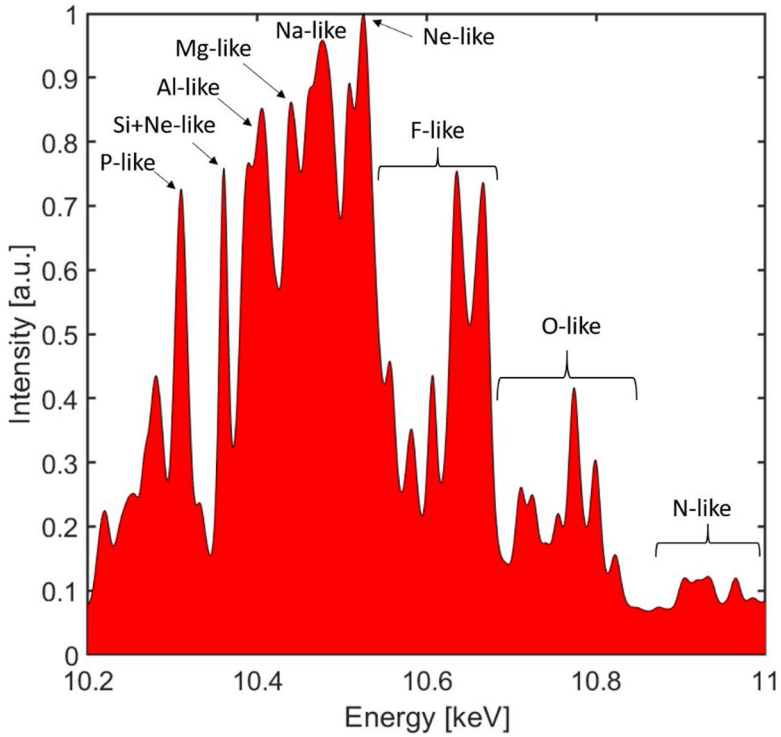

Extended Data Fig. 1 | Simulated Au spectrum. Simulated Au spectrum corresponding to solid flat gold target irradiated at an intensity of 4×10^{21} Wcm^{-2}. Best agreement with the experimental spectrum is obtained when lines from F-like to N-like Au are shifted down in energy by ~0.4%. Similar shifts were necessary in ref. [7] when comparing the calculated Au line energies with the measurement. The spectrum was computed using transient calculations performed with the atomic physics/hydrodynamic code RADEX using initial plasma parameters computed by the PIC simulations. The RADEX code uses detailed atomic data from the Hebrew University Lawrence Livermore Atomic Code (HULLAC) (ref. [25]). It was run using 200 to 1500 levels per ion from Cu-like (Au^{50+}) to B-like (Au^{74+}) to accurately simulate the large number of transitions from the L shell configuration. The simulated spectrum shows emission of all the observed lines for charge states from Ne-like to N-like Au.

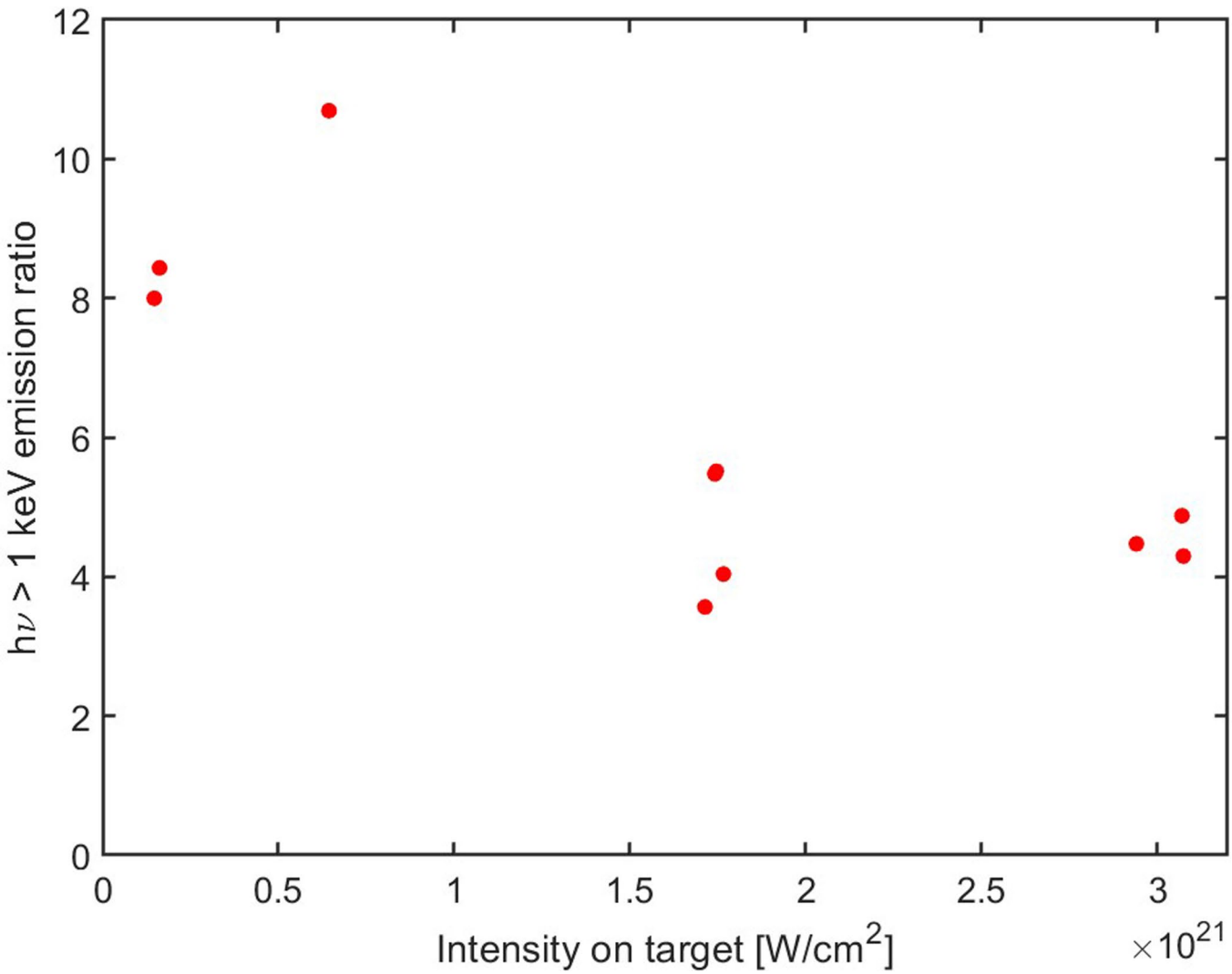

Extended Data Fig. 2 | Ratio of X-ray emission between nanowire and solid-density targets. Ratio of X-ray emission at photon energies > 1 keV from an Au nanowire target (100 nm diameter nanowire array, 15 % solid density) to Au solid foil target as a function of irradiation intensity.

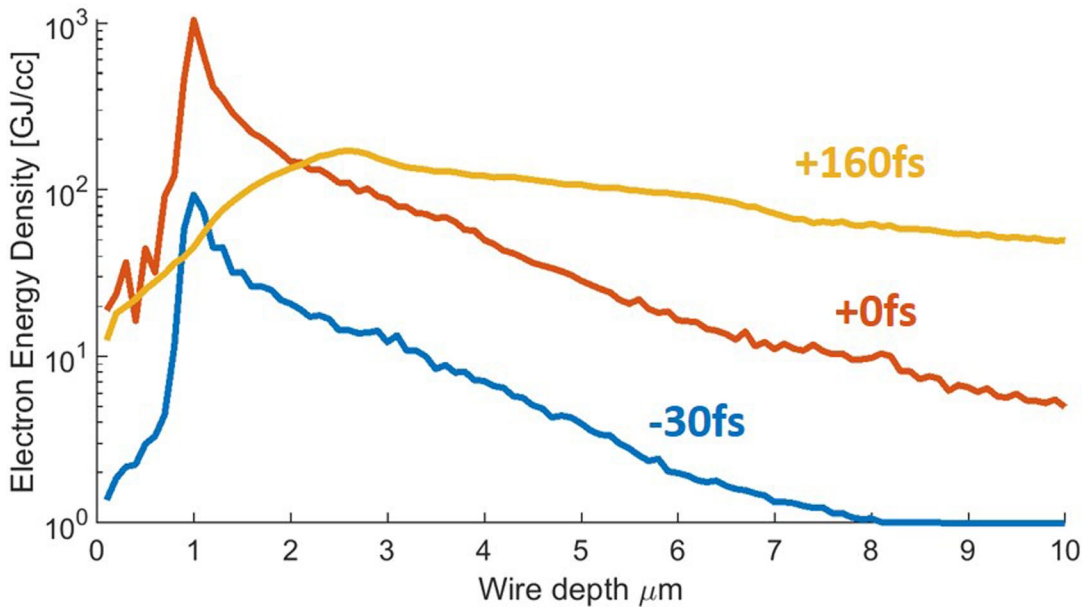

Extended Data Fig. 3 | Computed electron energy density. Computed electron energy density for an array of 100 nm diameter Au nanowire array (15% solid density) plotted for three different times with respect to the peak of the laser pulse (−30fs, 0 fs and +160 fs). Irradiation intensity 4×10^{21} Wcm^{-2}.

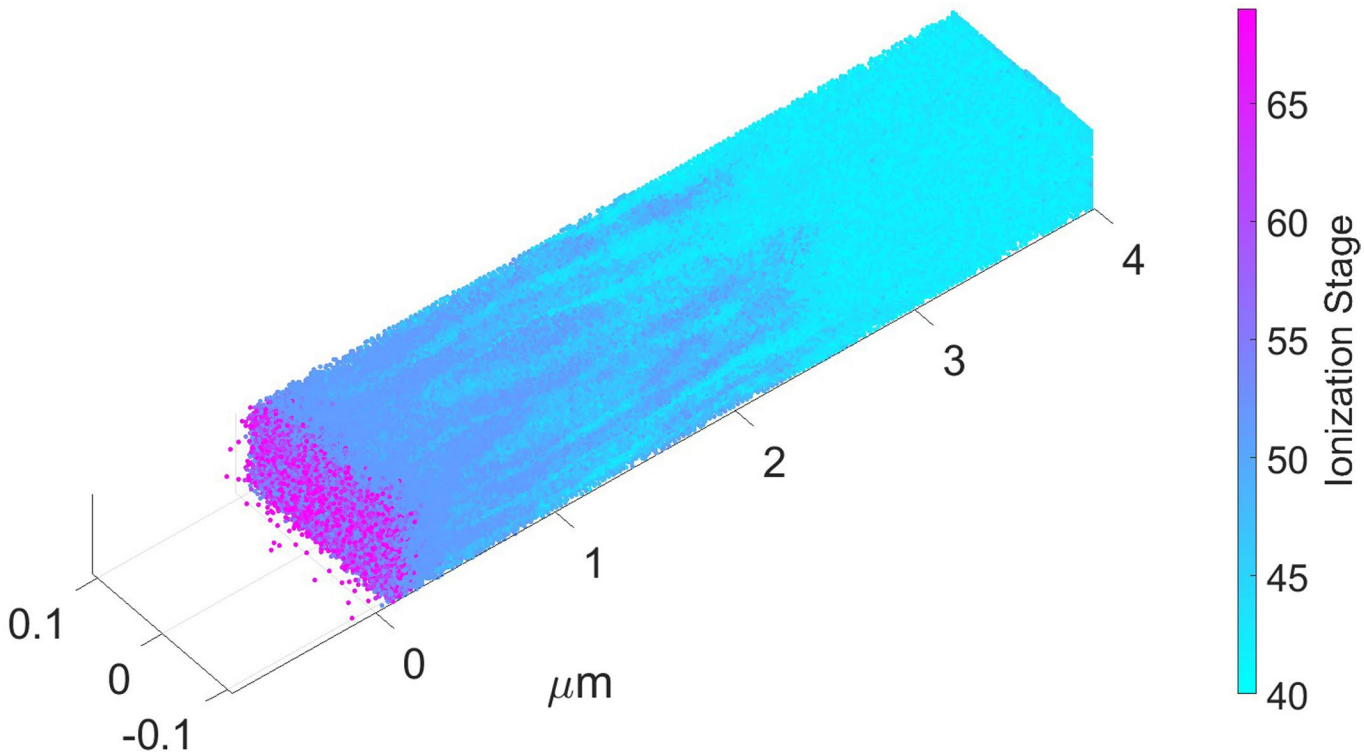

Extended Data Fig. 4 | High-resolution 3D particle in cell simulation of solid-density ionization. Predicted ionization stage for an infinite (periodically bounded in the transverse direction) solid Au flat target at +30 fs following the peak of the laser pulse.

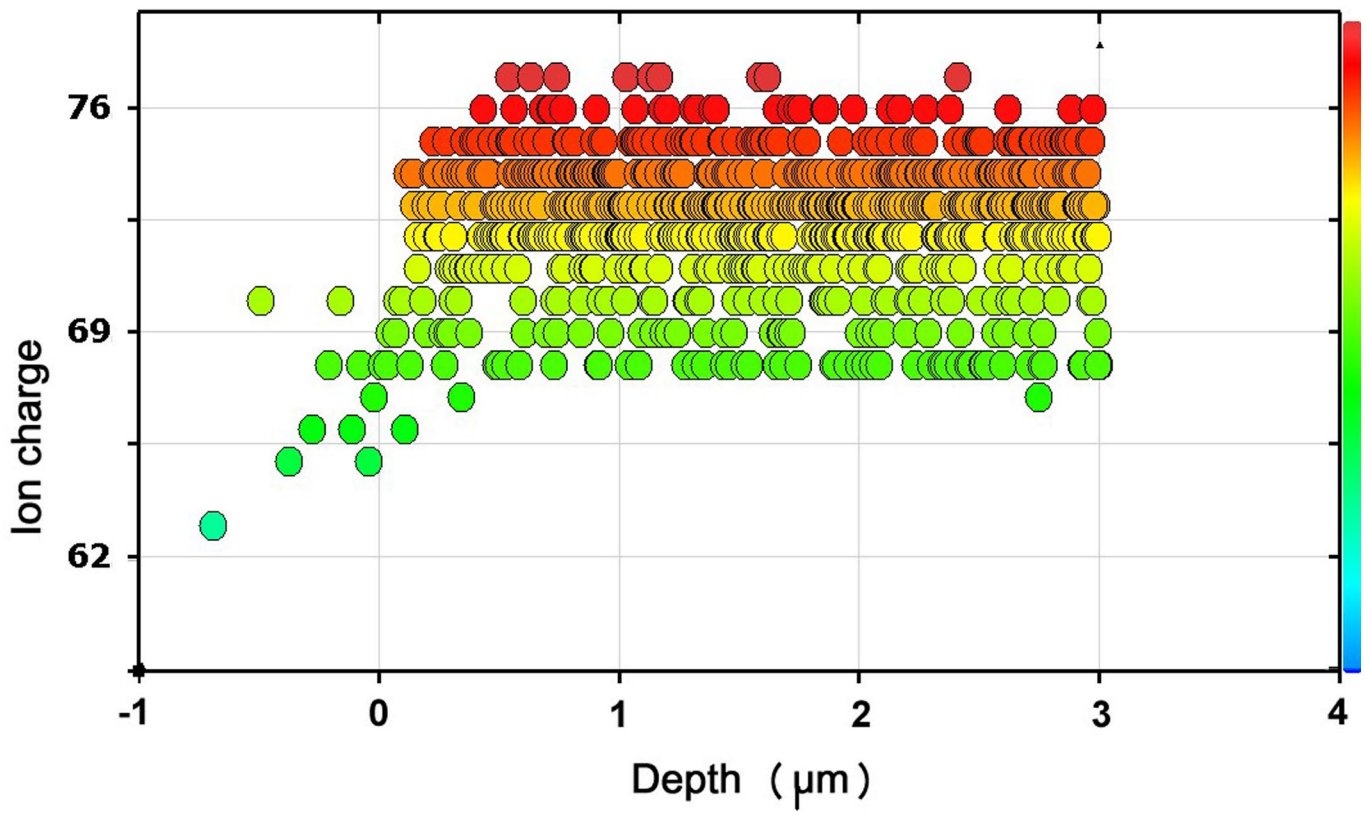

Extended Data Fig. 5 | Computed ionization for a 5 micron diameter laser spot. Computed ionization state as a function of target depth for a solid-density Au foil irradiated at an intensity of 4×10^{21} Wcm^{-2} with a 5 μm FWHM diameter focal spot showing atoms ionized up to He-like Au^{77+}.

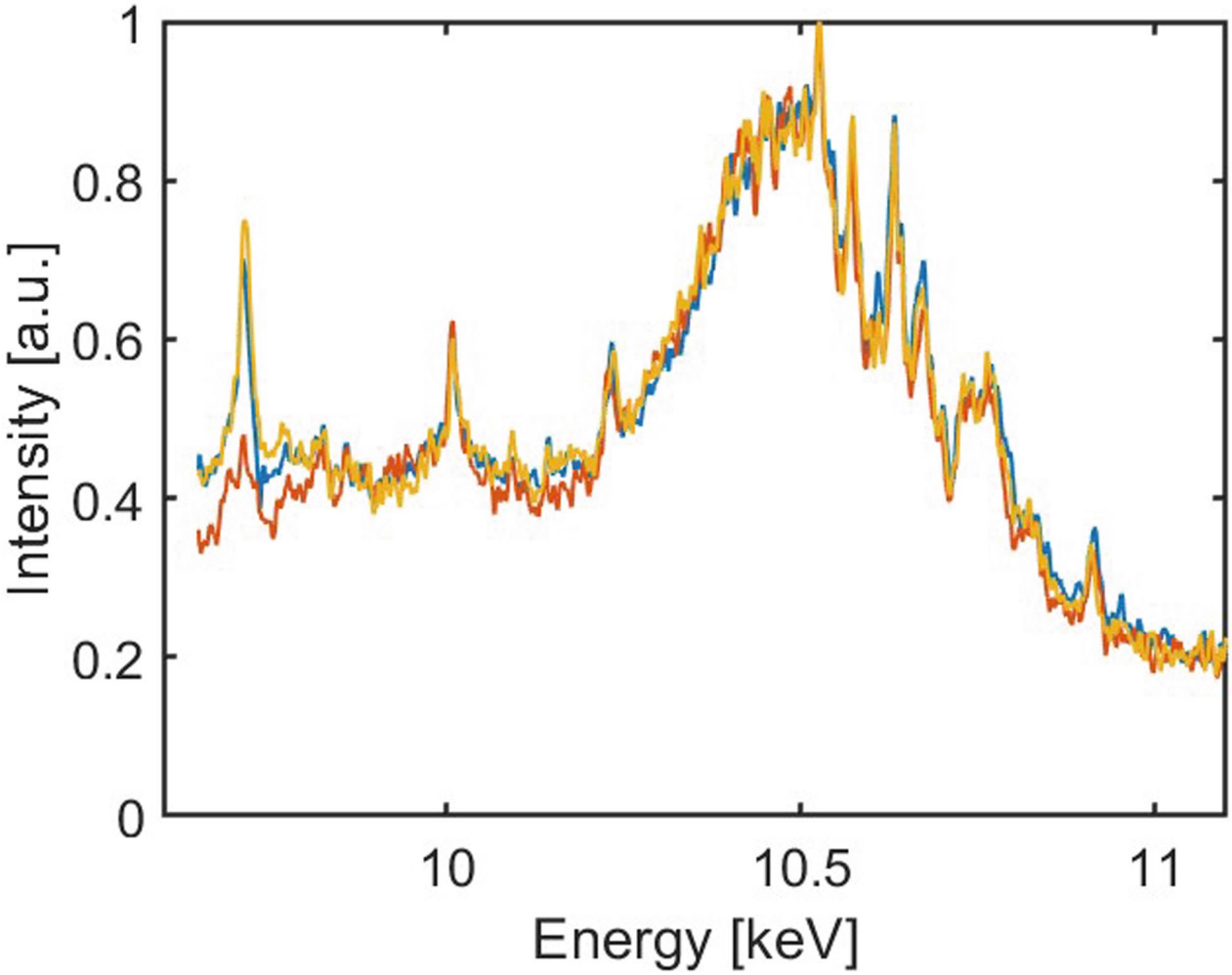

Extended Data Fig. 6 | Shot to shot reproducibility. Three consecutive single shot Au L shell spectra from an Au foil normalized by the Ne-like Au line emission showing good shot to shot reproducibility.

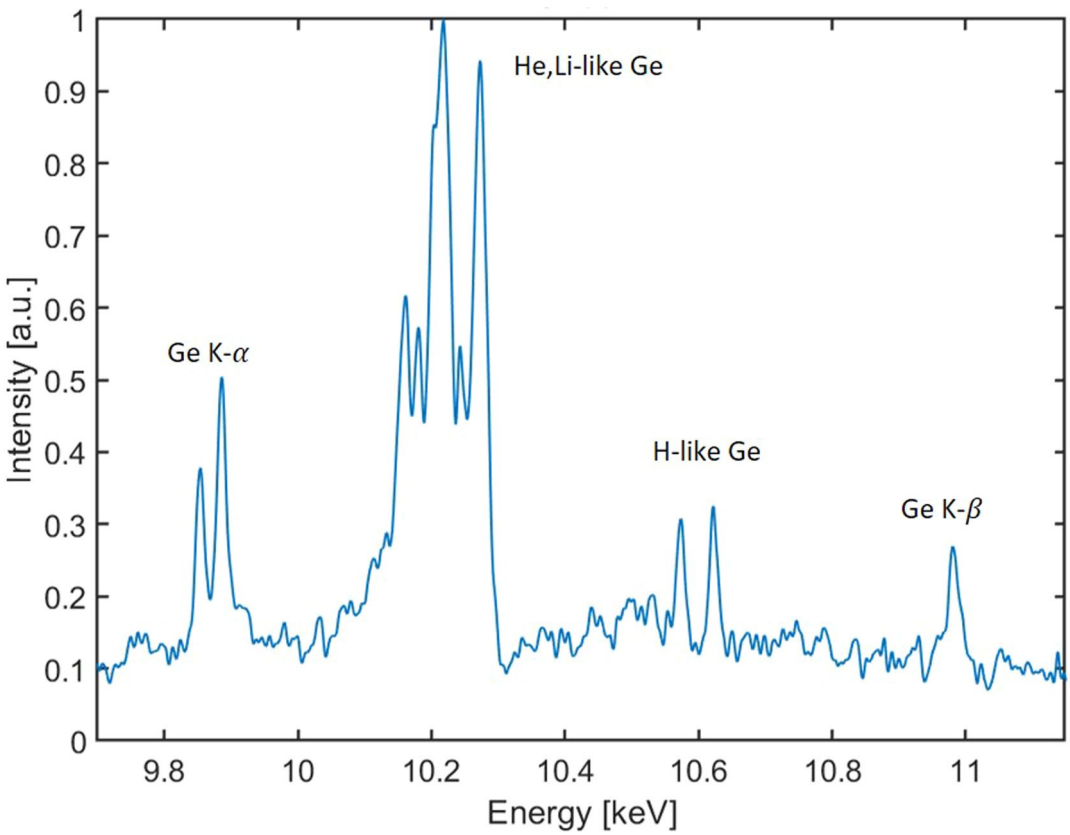

Extended Data Fig. 7 | Ge K-shell spectrum used to calibrate Au L-shell. K-shell spectrum of the Ge plasma used to calibrate the Von Hamos spectrometer in the 9.7–11.2 keV spectral range. The plasma was generated irradiating a 17 μm thick Ge wafer at an intensity of 3×10^{21} W cm^{-2}.

PHYSICS

Energy penetration into arrays of aligned nanowires irradiated with relativistic intensities: Scaling to terabar pressures

2017 © The Authors, some rights reserved; exclusive licensee American Association for the Advancement of Science. Distributed under a Creative Commons Attribution NonCommercial License 4.0 (CC BY-NC).

Clayton Bargsten,[1] Reed Hollinger,[1] Maria Gabriela Capeluto,[2] Vural Kaymak,[3] Alexander Pukhov,[3] Shoujun Wang,[1] Alex Rockwood,[4] Yong Wang,[1] David Keiss,[4] Riccardo Tommasini,[5] Richard London,[5] Jaebum Park,[5] Michel Busquet,[6] Marcel Klapisch,[6] Vyacheslav N. Shlyaptsev,[1] Jorge J. Rocca[1,4]*

Ultrahigh-energy density (UHED) matter, characterized by energy densities >1 × 10^8 J cm^{-3} and pressures greater than a gigabar, is encountered in the center of stars and inertial confinement fusion capsules driven by the world's largest lasers. Similar conditions can be obtained with compact, ultrahigh contrast, femtosecond lasers focused to relativistic intensities onto targets composed of aligned nanowire arrays. We report the measurement of the key physical process in determining the energy density deposited in high-aspect-ratio nanowire array plasmas: the energy penetration. By monitoring the x-ray emission from buried Co tracer segments in Ni nanowire arrays irradiated at an intensity of 4 × 10^{19} W cm^{-2}, we demonstrate energy penetration depths of several micrometers, leading to UHED plasmas of that size. Relativistic three-dimensional particle-in-cell simulations, validated by these measurements, predict that irradiation of nanostructures at intensities of >1 × 10^{22} W cm^{-2} will lead to a virtually unexplored extreme UHED plasma regime characterized by energy densities in excess of 8 × 10^{10} J cm^{-3}, equivalent to a pressure of 0.35 Tbar.

INTRODUCTION

Laboratory creation of matter in the ultrahigh-energy density (UHED) regime is of great interest for the realization of inertial confinement fusion (*1*, *2*), to further the understanding of atomic processes in astrophysical and extreme laboratory environments (*3*–*5*), and to generate intense sources of x-rays and high-energy particles (*6*, *7*). However, the creation of matter in this regime in the laboratory has been limited to the central hot spot of the spherically imploded capsule in inertial confinement fusion experiments conducted using the world's highest-energy lasers (*8*, *9*). The ability to create UHED matter using smaller facilities is thus of great interest to make this extreme plasma regime more accessible for fundamental studies and applications. One such application is the efficient conversion of optical laser light into bright flashes of x-rays, which requires the radiative lifetime of the plasma to be shorter than the hydrodynamic cooling time. This, in turn, demands simultaneously having a large collision rate (and therefore a large density of energetic electrons) and a large plasma size. However, heating a large UHED plasma volume is a challenge that even many of today's most powerful lasers fall short of achieving when irradiating solid slab targets. In this conventional heating scheme, the leading edge of the laser pulse rapidly creates a plasma blow-off, which prevents the remainder of the laser pulse from directly heating the solid region of the target. Heating by hot electrons using today's most energetic short pulse lasers has just surpassed the boundary into the UHED regime (for example, achieving 2 Gbar). For example, temperatures of 0.6 keV at a density of 1.5 g/cc were recently reported for a 0.15-μm-thick Al foil tamped by 10 μm of plastic on both sides, irradiated by 100-J pulses of 0.5-ps duration (*10*). Simulations indicate a pressure of 0.5 Gbar, and an energy density approaching 1 × 10^8 J cm^{-3} was obtained. Similar temperatures were achieved at a density of 9 g/cc, and therefore higher pressure and energy density, using diamond tamped Al targets compressed with a pair of 200-J, long laser pulses before the arrival of the short heating pulse (*10*). Several other experiments in which pulses of 0.35- to 2-ps duration irradiated plastic foils with buried metal layers reported similar temperatures (*11*–*14*). Heating with 400-J pulses of 0.8-ps duration achieved a 5-keV surface temperature decreasing to 0.6 keV at 1.3-μm depth (*15*).

Alternatively, irradiation of high-aspect-ratio vertically aligned nanowire arrays with ultrahigh-contrast femtosecond laser pulses of only joule-level energy provides a unique combination of nearly complete optical absorption and drastically enhanced light penetration into near-solid density targets, allowing the material to be volumetrically heated deep into the UHED regime. Other types of structured targets have also been successfully used to increase absorption, as evidenced by enhanced x-ray emission from "smoked" targets (*16*), nanospheres (*17*), gratings (*18*, *19*), and "velvet" nanowire targets (*20*–*23*). However, high-aspect-ratio vertically aligned nanostructures with vacant spaces surrounding them are unique in allowing for the deep penetration of ultrafast optical laser pulse energy into the material, where light is trapped and practically totally absorbed (*24*). Electrons ripped off the nanowire surface by the large laser field are accelerated to acquire high energy in the voids. Collisions of these energetic electrons with the nanowires rapidly heat the material to extreme temperatures, causing the nanostructures to explode and rapidly fill the voids. When the gaps are filled with plasma, a continuous critical electron density layer that forbids further coupling of laser energy into the material is formed. The use of sufficiently short laser pulses allows for very efficient coupling of the pulse energy deep into the nanowire array, heating a large volume of near-solid-density material several micrometers in depth to multi–kilo–electron volt temperatures. This new approach to volumetric heating opens access to the UHED plasma regime using tabletop, joule-class, femtosecond lasers.

[1]Electrical and Computer Engineering Department, Colorado State University, Fort Collins, CO 80523, USA. [2]Departamento de Física, Universidad de Buenos Aires, Buenos Aires, Argentina. [3]Institut für Theoretische Physik, Heinrich-Heine-Universität Düsseldorf, 40225 Düsseldorf, Germany. [4]Physics Department, Colorado State University, Fort Collins, CO 80523, USA. [5]Lawrence Livermore National Laboratory, Livermore, CA 94551, USA. [6]ARTEP Inc., Ellicott City, MD 21042, USA.
*Corresponding author. Email: jorge.rocca@colostate.edu

Downloaded from http://advances.sciencemag.org/ on January 12, 2017

Considering that the aligned nanowire arrays are highly optically absorbent, the heat penetration depth into the arrays is the key unknown parameter for determining the plasma volume heated and, thus, the deposited energy density. Here, we report the first definitive measurement of the volume of heated material in arrays of high-aspect-ratio aligned nanowires irradiated by femtosecond pulses of relativistic intensity. We present the results of experiments at an intensity of 4×10^{19} W cm^{-2} that show heating of near-solid-density matter to multi–kilo–electron volt temperatures over depths of several micrometers. The results serve to validate a model of the relativistic interaction that is used to study the physics of these unique plasmas and to predict the UHED conditions that will be achieved when the intensity is increased to the limit of currently available laser systems and beyond. As shown below, this approach promises to achieve unprecedented energy densities in excess of 8×10^{10} J cm^{-3}, equivalent to 0.35-Tbar pressures using existing ultrafast laser facilities.

The measurement technique consists of monitoring the He-α line emission from buried nanowire segments of a selected tracer material. This required growing arrays of ordered nanowires that have a compositional change along the length of each nanowire (Fig. 1, A and B). We found it advantageous to choose neighboring elements on the periodic table that have similar ionization dynamics for the top and buried (tracer) segments to form an array that does not differ significantly from one of uniform composition. This selection also allows the characteristic spectral lines of both materials, such as the He-α lines, to be recorded simultaneously within the spectral window of a single crystal spectrometer. In this experiment, the composition of the top segment of the nanowires was nickel (Z = 28), and the buried tracer element was cobalt (Z = 27). The experiments were simulated using the combination of a relativistic three-dimensional (3D) particle-in-cell (PIC) code in combination with a transient atomic kinetics and radiation transport model.

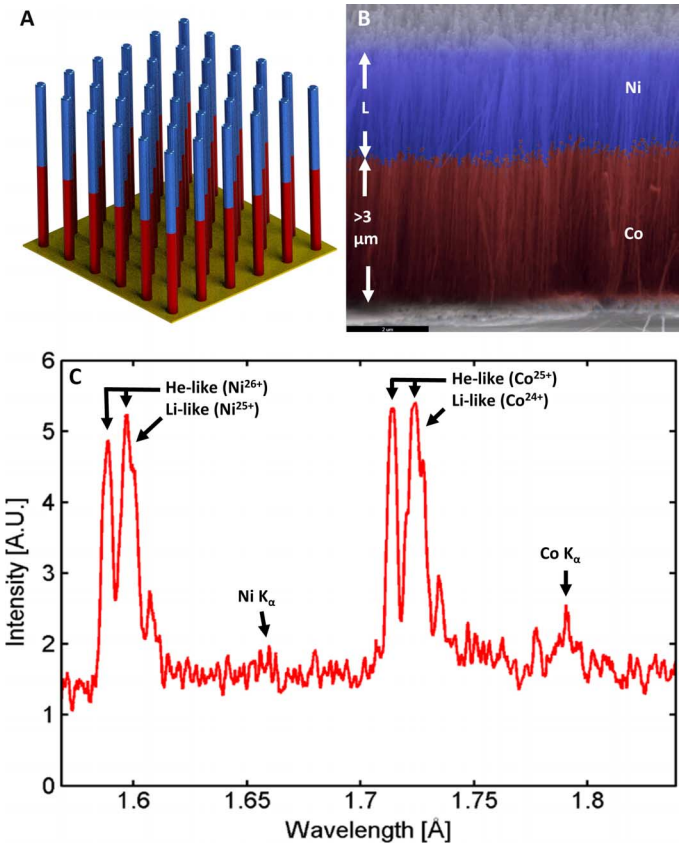

Fig. 1. Schematic diagram, composition map, and x-ray spectrum of a two-composition Ni-Co nanowire array. (**A**) Schematic diagram of segmented two-composition Ni-Co nanowire array. The top Ni segment ranges in length from 1 to 6 μm. The nanowires are 55 nm in diameter and form an array that is 13% of solid density. (**B**) Scanning electron microscopy image with energy-dispersive spectroscopic elemental composition measurement indicating the concentration of Ni (blue) and Co (red). (**C**) Example spectra showing the He-like line dominance over the K$_\alpha$ lines for the two elements as recorded using a von Hamos crystal spectrometer. A.U., arbitrary units.

RESULTS AND DISCUSSION

The experiments were conducted by irradiating the segmented nanowire arrays with λ = 400 nm, ultrahigh-intensity contrast (>10^{12}) pulses of 0.6 J of energy, and 55-fs full width at half maximum (FWHM) duration from a frequency-doubled titanium-sapphire laser at Colorado State University (see Materials and Methods). The ultrahigh contrast is crucial to preserve the nanowires until the arrival of the intense laser pulse. The laser pulses were focused onto the nanowire arrays using an f/2.7 parabolic mirror. The emitted x-ray radiation was analyzed using a von Hamos crystal spectrometer (*25*) in which a mica crystal spectrally disperses the signal onto a 2D back-thinned charge-coupled device (CCD) sensor array.

Figure 1C shows a single-shot spectrum from an irradiated dual composition Ni-Co nanowire array in which the He-like lines of the Ni and Co segments were simultaneously recorded. Both materials have a high Young's modulus, which facilitates the growth of arrays of well-aligned, high-aspect-ratio nanowires. The nanowire arrays were grown by sequential electrodeposition of the selected metals into porous anodic aluminum oxide membranes. Subsequent dissolution of the membranes results in freestanding aligned nanowire arrays (see Materials and Methods). The compositional change was thus created by first growing 3- to 4-μm-long Co nanowires at the base of each array followed by the growth of segments of Ni of several selected lengths on top. The change in composition along the nanowires is visible in the scanning electron microscope energy-dispersive spectroscopy (EDS) measurement shown in Fig. 1B. The arrays used in the experiment consisted of 55-nm- diameter nanowires spaced such that the array had an average atomic density corresponding to 13% of solid density.

Figure 2 shows a series of measured spectra resulting from irradiating Ni-Co nanowire targets in which the top wire segment of Ni increases in length from 1.5 to 5 μm. The spectra show an increase in the He-like Ni line emission signal and a corresponding decrease in the He-like Co signal as the length of the top Ni nanowire segment increases. In the case of the array with a 1.5-μm-long top Ni layer, the Co lines dominate. This is a first clear indication that the heat penetrates more than 3 μm along the length of the nanowires. A decrease in intensity of the Co lines is subsequently seen as the length of the top nickel layer is increased. The emission from He-like Co ions is observed for targets with up to 4 μm of Ni on top. As the top nickel layer reaches 5 μm in thickness, the Co lines decrease in intensity to a level near that of the continuum background signal that results from bremsstrahlung and radiative recombination. In agreement with the simulations discussed below, this demonstrates that sufficient heat to ionize Co ions to the He-like stage penetrates at least 4-μm-deep into the near-solid-density material. Figure 3 plots the measured peak intensity of the Co and Ni He-α lines as a function of Ni nanowire segment length. The Ni lines become stronger as the

Downloaded from http://advances.sciencemag.org/ on January 12, 2017

length of the top segment of this material is increased up to 3 to 4 μm, the length beyond which their strength saturates. Simultaneously, the strength of the Co lines decreases until they disappear into the continuum when the Ni segments reach 5 μm in length.

Simulations of the x-ray emission spectra of arrays with top Ni segments of different length were conducted with a transient atomic kinetics and radiation transport model that uses the electron energy distribution computed by the relativistic 3D PIC simulations (see Materials and Methods). The synthetic spectra (Fig. 4, top) closely replicate the observed features of the experimental data. The bottom panel of Fig. 4 illustrates the agreement between the measured and simulated Co/Ni line ratios as a function of Ni wire segment length. Figure 5 shows the simulated spatial distribution of He-like Ni and Co ions for an array with a top segment of 3-μm Ni nanowires after the peak of the laser pulse. It illustrates the generation of He-like Co ions several micrometers under the top Ni nanowire layer. The agreement between measurement and simulations validates the model, which is used below to predict the plasma conditions that could be obtained by increasing the irradiation intensity.

The energy density and pressure for hot electron gases are given by integrals of the energy and momentum-velocity product, weighted by the distribution function. We have calculated the energy density directly from the particle data from the PIC simulation and estimated the pressure from that, using a formula for an equilibrium relativistic gas, accurate to 1% (see Materials and Methods) (*26*). Computed maps of the kinetic energy density at four different times during the plasma evolution are shown in Fig. 6. Optical-field ionization (OFI) is observed to begin the heating process at the nanowire surface, with the strong electric field of the laser pulse stripping electrons and creating ionization states up to $Z = 18$. The electrons are rapidly accelerated into the gaps. Collisional electron impact ionization produces higher ionization states as the hot electron population deposits its energy deep into the nanowire cores. The electrons stripped from the wires are accelerated toward the substrate. Charge balance demands the generation of a large laser-induced return current through the nanowires. The resulting strong quasi-static self-generated azimuthal magnetic field pinches the

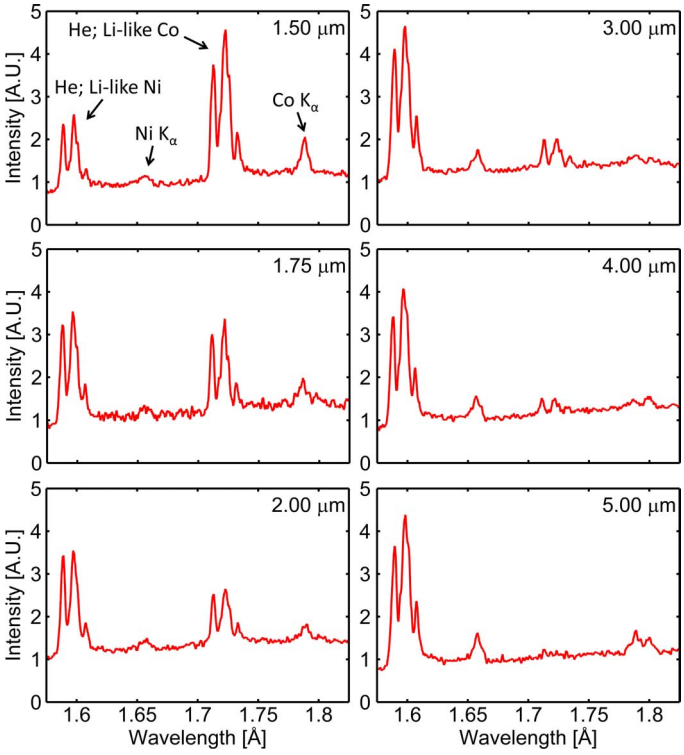

Fig. 2. Measured spectra of Ni-Co–segmented nanowire arrays with different lengths of Ni wires (listed in the top right corner of each plot) on top of cobalt wires, irradiated by 55-fs pulses at an intensity of ~4 × 10^{19} W cm^{-2}. The vertically aligned wires are 55 nm in diameter and form an array that has an average atomic density that is 13% of solid density. Lines of He-like and Li-like Ni and Co are visible along with their respective K_α lines.

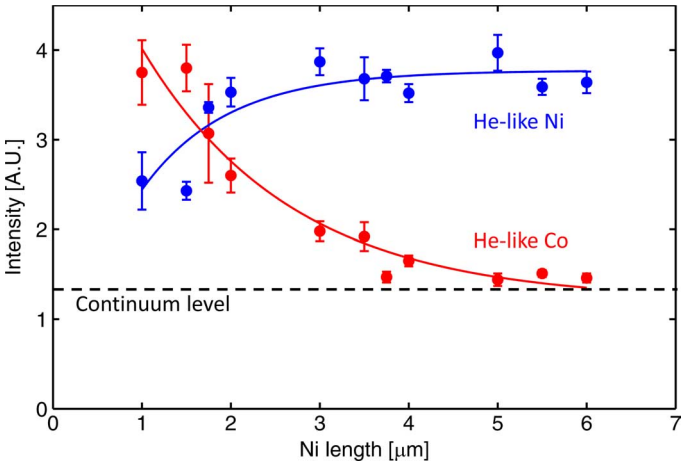

Fig. 3. Measured intensities of the He-like Co and Ni lines as a function of the length of the top Ni nanowire segment. The target and laser parameters are the same as those in Fig. 2.

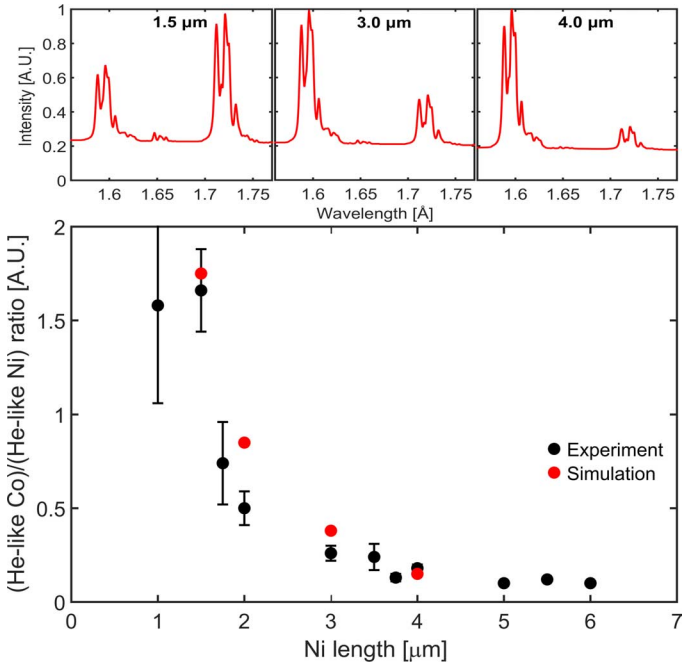

Fig. 4. Simulated spectra corresponding to arrays with different wire lengths used in the experiment are shown in the top three plots. The target and laser parameters are the same as those in Fig. 2. Measured and simulated (Co He-α)/(Ni He-α) line ratios as a function of Ni nanowire segment length are shown on the bottom.

Downloaded from http://advances.sciencemag.org/ on January 12, 2017

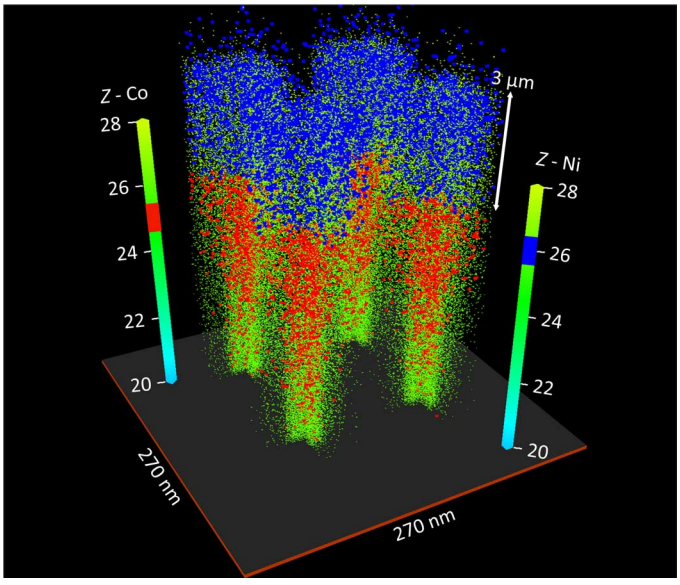

Fig. 5. PIC simulation of the density of He-like ions in an array composed of segments of vertically aligned Ni and Co nanowires (blue, He-like Ni; red, He-like Co). The target and laser parameters are the same as those in Fig. 2. The top Ni wires are 3.0 μm in length. The laser pulse impinges from the top at normal incidence to the array.

nanowires into a hot, extremely dense plasma (*27*). A plasma density surpassing 10^{24} cm^{-3} with an energy density of 22 GJ cm^{-3} and pressure of 125 Gbar is quickly reached within the wires near their tips (+4-fs frame; Fig. 6). The laser pulse continues to propagate down the length of the wires and deep into the array as long as the interwire gaps remain free of dense plasma. As the wires expand, the interwire gaps are filled with a supercritical-density plasma. Collisions homogenize the plasma, creating a uniform plasma layer several micrometers thick in which the atoms are ionized up to the He-like stage observed in the measurements. In the two earliest frames in Fig. 6 (+4 and +44 fs), the wire tips appear to be loosely connected by regions of higher energy density. This is a result of the array geometry in which the gaps are narrower in the directions directly between wires. These narrower gap regions thus fill with particles more quickly and reach higher-energy densities faster than the diagonal regions. Expansion of the wires continues to progressively close the interwire gaps along the length of the wires (+124-fs frame; Fig. 6) until the whole target cross section is filled with material at an energy density of 1 GJ cm^{-3} and pressure of 7 Gbar (+304-fs frame; Fig. 6). A thermalized electron temperature of ~14 keV is reached over the plasma volume with an average electron density greater than 3×10^{23} cm^{-3}. Even higher plasma densities can be obtained by irradiating arrays with higher wire filling factors, arrays made of a higher Z material, or a combination of both. As an example in the Supplementary Materials, we include a spectrum of a Ni nanowire target with an average atomic density corresponding to 30% of solid density irradiated at an intensity of 4×10^{19} W cm^{-2} (fig. S1). The spectrum is again dominated by He-like (Ni^{+26}) and Li-like (Ni^{+25}) lines, which indicate the high degree of ionization is maintained. In this case, the average electron

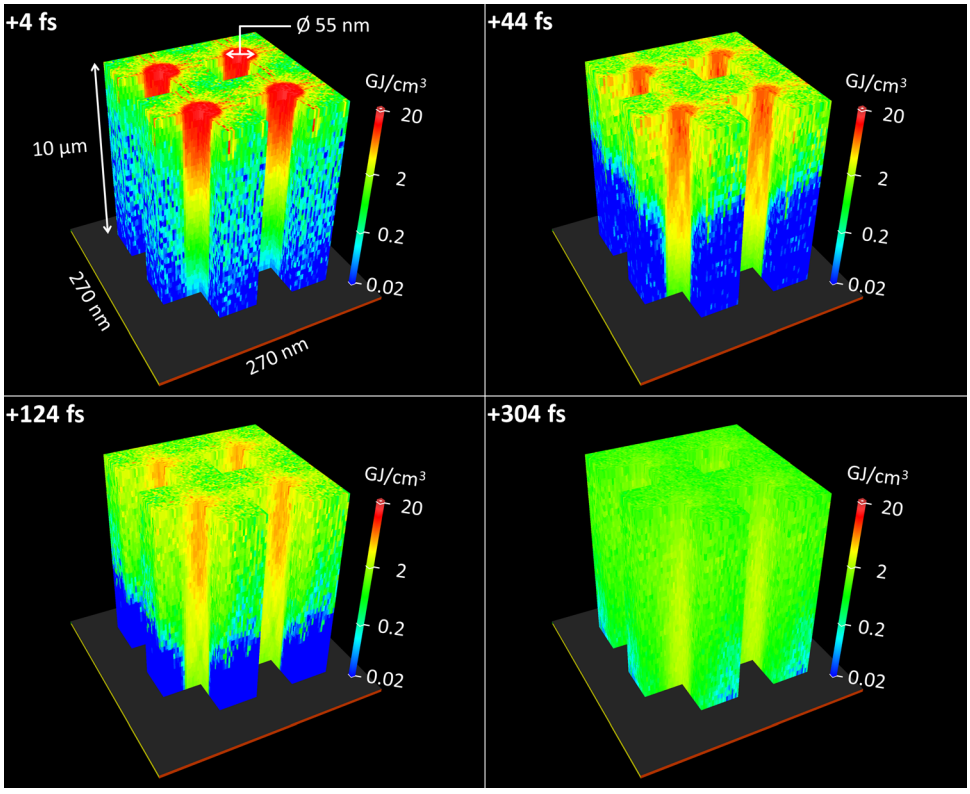

Fig. 6. ED distribution computed by PIC simulation. The target and laser parameters are the same as those in Fig. 5. Each frame corresponds to a different time with respect to the peak of the laser pulse as indicated by the time stamp in the top left corner of each frame. The laser pulse impinges into the array from the top at normal incidence.

Downloaded from http://advances.sciencemag.org/ on January 12, 2017

density of the homogenized plasma increases up to ~7 × 10^{23} cm^{-3}, nearly 100 times the critical density.

We conducted additional PIC simulations to predict the plasma conditions that could be achieved by further increasing the laser irradiation intensity to 1 × 10^{22} W cm^{-2} (a_0 = 34). The results suggest the generation of unprecedented energy densities and pressures. This is illustrated in Fig. 7 for an array of 400-nm-diameter Au nanowires with an average atomic density corresponding to 12% of solid density, irradiated with a 30-fs duration pulse. The plasma density in the gold nanowires during the nanoscale pinch compression phase reaches 2 × 10^{25} cm^{-3}, which corresponds to nearly 3200 times the critical density (fig. S2). Other laser-target configurations could reach even higher densities during the nanopinch (for example, 6 × 10^{25} cm^{-3}). These extreme peak densities would approach those obtained from fusion hot spots using megajoule laser energies at the National Ignition Facility (~1 × 10^{26} cm^{-3}) (*28*) while potentially reaching higher temperatures. The energy density within the nanowires is predicted to reach a peak value of 2 TJ cm^{-3}, equivalent to a pressure of 7 Tbar near the end of the laser pulse (+21-fs frame; Fig. 7). The expansion of the heated nanowires is computed to create a plasma layer in which the energy density is 80 GJ cm^{-3}, equivalent to a 0.35-Tbar pressure (+500-fs frame; Fig. 7), larger than the solar interior pressure. The electron energy can be described by a two-temperature distribution, which rapidly thermalizes into a single-temperature distribution defined by an electron temperature of ~500 keV, 500 fs after the peak of the laser pulse (see fig. S3).

Figure 8 shows that the gold atoms are predicted to reach extreme degrees of ionization. At 20 fs after the peak of the laser pulse, Ni-like Au ions are dominant, whereas ions up to Ne-like (Au^{+69}) are also predicted to be present within the nanowires for depths up to several micrometers. A few hundred femtoseconds after the end of the laser pulse (for example, +500 fs in Fig. 7), the plasma is still hot, and ionization still continues, creating charge states up to Au^{+70}. Moreover, irradiation of an array of 150-nm-diameter Au nanowires with an initial average density of 30% solid is predicted to result in denser plasma in which Au atoms near the tip of the array could potentially be ionized to the Be-like stage (Au^{+75}). Irradiation of higher Z elements is expected to result in even higher charge states.

These extreme energy densities offer important advantages for the efficient generation of ultrashort pulses of x-rays and neutrons. In the case of x-ray generation, the large plasma density decreases the radiative lifetime. This results in an increase in the hydrodynamic-to-radiative lifetime ratio that leads to a large increase in conversion efficiency. Accordingly, in experiments we have conducted with aligned gold nanowires, we have measured a record conversion efficiency into ultrashort pulses of >1-keV photons of 10% in 2π str. In the case of the generation of neutrons by deuterium-deuterium or deuterium-tritium fusion reactions, the high density of energetic ions is an important advantage because the reaction rate is proportional to the square of the density. These aligned nanostructure plasmas share some similarities to the efficient volumetric heating of clusters in a supersonic gas

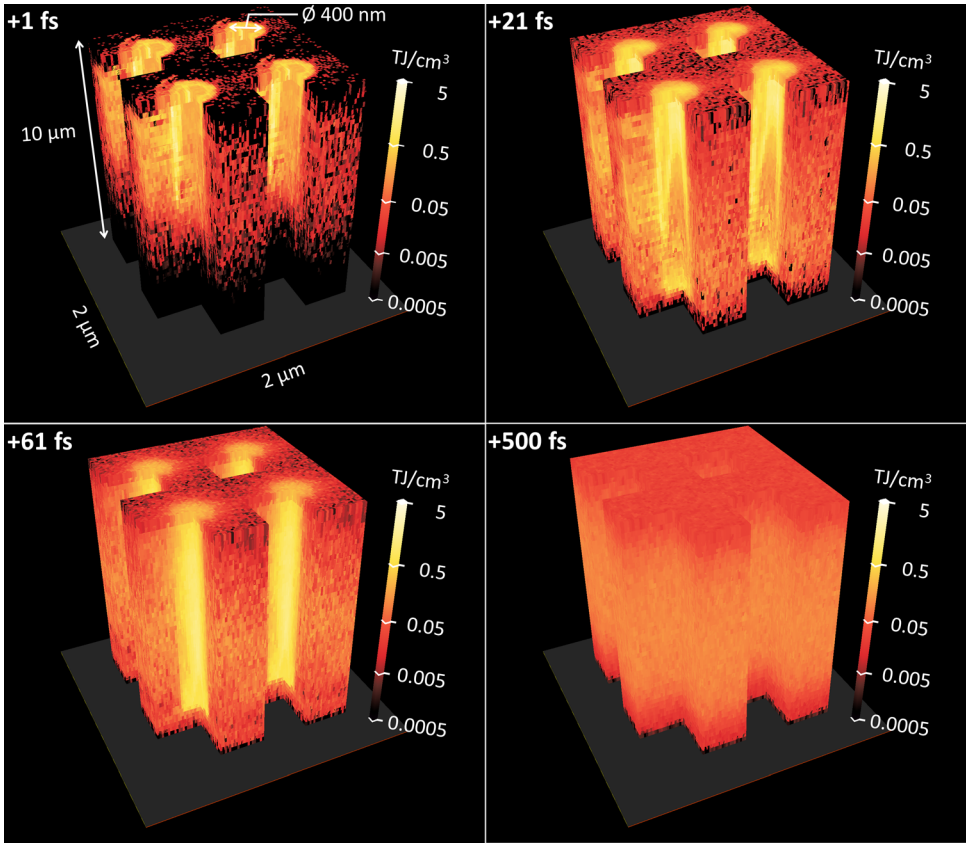

Fig. 7. PIC-simulated energy density distribution in an array of vertically aligned 400-nm-diameter Au nanowires irradiated with an intensity of 1 × 10^{22} W cm^{-2} (a_0 = 34) using a 400-nm wavelength pulse of 30-fs duration. The average atomic density is 12% of solid density. Each frame corresponds to a different time with respect to the peak of the laser pulse. The laser pulse impinges into the array from the top at normal incidence.

Downloaded from http://advances.sciencemag.org/ on January 12, 2017

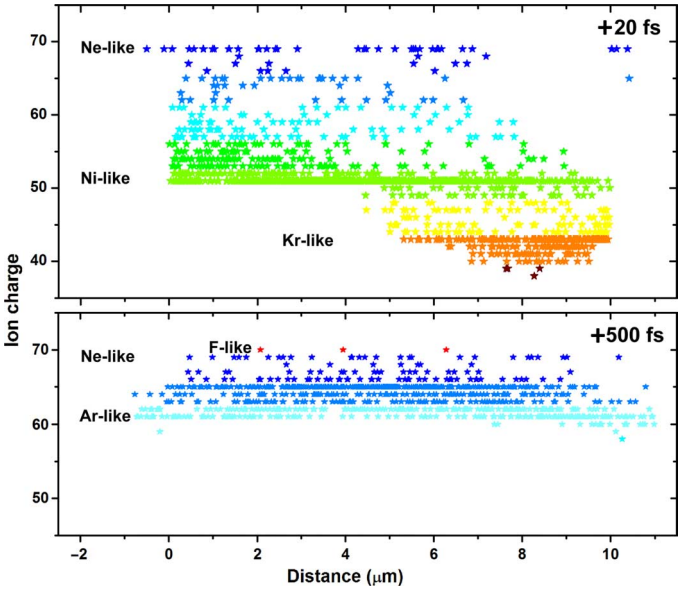

Fig. 8. Ion charge distribution as a function of depth for an array of 400-nm-diameter Au nanowires with 12% of solid density, irradiated at an intensity of 1 × 10^{22} W cm^{-2} as in Fig. 7. This plot was obtained by randomly choosing a fraction of the ions and placing a star at each charge and position. Groups of ionization stages are assigned different colors (for example, Z = 66 to 70 is blue) to accentuate the ion distribution and identify rare ions, such as the F-like ions in the bottom.

jet (*29*), but with the additional advantage of having several orders of magnitude higher-average density, potentially leading to record fusion neutron yields with compact lasers.

It is also of interest to gain insight into how the energy density scales with irradiation intensity. However, this scaling would have a very limited range of applicability without the simultaneous change of the nanostructure target parameters, for example, the nanowire diameter. The ideal configuration for many applications, such as neutron generation, efficient conversion into x-rays, and creation of highest-Z ions, requires obtaining a plasma lifetime as large as possible compared to the characteristic times of the fusion reactions, radiation cooling, and ionization time, respectively. That means that the laser energy deposition depth has to be typically of the order of the laser focal spot size, which, in our case, is 4 to 6 μm. As the irradiation intensity is increased, scaling of the interwire distance is required to maintain this constant energy penetration depth. Otherwise, not only would the laser energy penetration depth be either too short or too long, but the efficiency of the laser energy deposition would also decrease. This is because there exists a time for the closure of the interwire space for the laser by the expanding plasma, after which a continuous critical density layer is formed, which increases the fraction of laser energy reflected (*24*). Therefore, to determine the energy density scaling, we used the strategy of keeping the energy penetration depth approximately constant and comparable to focal spot size while scaling the interwire spacing and nanowire diameter (the latter is required to keep the average atomic density constant). For this case of approximately constant energy deposition depth, the peak value of the energy density occurring near the end of the laser pulse is computed to scale approximately linear with intensity I, energy density α I (see fig. S4). In comparison, at later times when the nanowires are completely dissolved into a homogeneous plasma, the energy density behaves as a sublinear function of the laser intensity, energy density α $I^{0.5}$, because of the faster thermal spread of the hotter plasma at larger intensities.

In conclusion, these results open a path to obtaining unprecedented pressures in the laboratory with compact lasers for the study of high energy density physics, high ionization states of high-Z atoms in high-density plasmas, and effects of opacities at ultrahigh pressures, temperatures, and densities. The experimentally validated numerical model predicts that experiments at an increased intensity of 1 × 10^{22} W cm^{-2} will result in the generation of unprecedented Tbar-level pressures in laboratory plasmas, surpassing even those in spherical compression laser fusion experiments. These plasmas can lead to record conversion efficiency of optical laser light into ultrafast x-ray flashes and to the efficient production of ultrafast neutron pulses by fusion in near-solid-density plasmas.

MATERIALS AND METHODS

Experimental setup

The dual-composition segmented nanowire array targets were irradiated with 400-nm wavelength, 0.6-J energy laser pulses of 55-fs FWHM duration from an ultrahigh-contrast frequency-doubled titanium-sapphire laser. The ultrahigh contrast, which is necessary to prevent destruction of the nanowires before the arrival of the main pulse, was achieved by frequency doubling with an 800-μm-thick type 1 potassium dihydrogen phosphate crystal. The 400-nm second harmonic light was separated from the 800-nm fundamental beam using a series of four highly selective dichroic mirrors. These high-contrast pulses were focused to an ~5-μm-diameter spot using a 90° off-axis parabolic mirror to achieve intensities of (4 ± 1) × 10^{19} W cm^{-2} on target. The focal spot size was determined by imaging with a 10× objective onto a 12-bit CCD camera. The laser pulse duration was measured using a single-shot frequency-resolved optical gating. The laser prepulse contrast in the picosecond range was monitored with a third-order scanning autocorrelator, and in the nanosecond range, it was determined using a photodiode and a set of calibrated neutral density filters. The prepulse intensity contrast of the frequency-doubled pulse was inferred to be greater than 1 × 10^{12}. The laser pulse energy was monitored on a shot-by-shot basis by measuring the reflection from a 500-μm-thick, 1% reflecting, multilayer-coated beam splitter placed before the off-axis parabola.

The emitted x-ray spectrum was measured using a von Hamos crystal spectrometer (*25*). The spectrometer used the third-order reflection from a cylindrically bent mica crystal to spectrally disperse the x-ray signal onto a back-thinned 2D CCD sensor. The sensor was shielded from electromagnetic noise and visible light by an electrically and optically sealed Faraday cage, in which the diffracted x-ray signal reaches the CCD through a 12.5-μm-thick Al foil filter. The thickness of the Al foil filter was selected to also stop lower-order reflections from the mica crystal.

Vertically aligned nanowire arrays

The nanowire arrays were grown by the electrodeposition of metallic ions into porous alumina templates. The density of pores determined the average density of the nanowire array. A Watts bath (*30*) solution was used for the deposition of both nickel and cobalt materials. This galvanostatic electrodeposition allowed for the wires to be grown to a desired length inside the template pores. As the buried tracer experiments required the wires to consist of segments of two different materials, Co was first deposited in the pores to a length of 3 to 4 μm,

Downloaded from http://advances.sciencemag.org/ on January 12, 2017

followed by subsequent deposition of Ni at variable lengths between 1 and 6 μm. High-resolution transmission electron microscope dispersive x-ray spectroscopy (EDS analysis) revealed that the junction region between the Co and Ni layers was smaller than 100 nm in length. Once the deposition was complete, wires were freed from the template through a dissolving process in 4 M NaOH. EDS from a scanning electron microscope was used to measure the elemental composition of the array along the length of the nanowires in each array (Fig. 1B).

Simulation tools

The relativistic 3D Virtual Laser Plasma Laboratory code (*31*) was used for the PIC simulations. The capabilities of its standard algorithms were extended by adding packages for OFI and binary collisions, including electron impact ionization. OFI was treated as an under-barrier tunneling phenomenon in the static electric field (*32*, *33*), with only sequential field ionization considered. The probabilities for Coulomb collisions between all particles in one mesh cell were calculated by a binary collision package. PIC simulations used a 3D geometry and self-consistently included ionization physics for both the Ni and Co atomic species present in the dual-composition target and for Au. A linearly polarized plane wave with 400-nm wavelength and Gaussian time envelope $a(t) = a_0 \exp(-t^2/\tau^2)$ was used to simulate the laser pulse where the normalized vector potential $a_0 = eA/mc^2 = 2.16$ corresponds to a laser intensity of $I_0 = 4 \times 10^{19}$ W cm^{-2} and a 55-fs FWHM pulse duration. The laser pulse was assumed to impinge on the nanowire array at normal incidence. The PIC simulation space consisted of a cell volume encompassing the wires and interwire gaps, as well as a space above the array to allow for expansion of the wire material as it exploded and thermalized. The simulation described all phases of the laser interaction with the nanowire array and subsequent explosion and thermalization. The code accounted for local field enhancements, field fluctuations, and resonance heating. However, bulk resonances were not considered to be present because of the average density that was higher than the critical density and the spacing of the nanowires that was smaller than the wavelength of the laser.

Simulations were also conducted with two postprocessor atomic models based on the code Radex (*34*) using atomic data from the HULLAC code (*35*). The first of these atomic models was used to compute the intensity ratio of Co/Ni He-like lines. It used the exact particle energy distribution computed with the PIC code. The second model, used to simulate the spectra (Fig. 4, top), was a very detailed atomic code that considered a large number of excited levels from all the ionization stages present. This greatly more computational intensive model used a two-temperature approximation to the electron energy distribution computed by the PIC code. Lines were computed taking into account the natural, Doppler, collisional, and Stark broadening. The Biberman-Holstein approximation (*36*, *37*) was used for radiation transport of the He-α lines. For comparison with experiments, instrumental broadening was added to the synthesized spectra (Fig. 4). The continuum was simulated by simple approximations for bremsstrahlung and radiative recombination radiation.

Estimation of the pressure from the energy density

The relationship between energy density and pressure could be readily calculated in the equilibrium case, where the distribution function was a relativistic Maxwellian, and in the nonequilibrium ultrarelativistic case, where the particle velocities were all near the speed of light. The result for an equilibrium relativistic gas is given by Synge (*38*). We used a simple approximation, accurate to 1%, given by Ryu *et al.* (*26*).

Defining β as the ratio of kinetic energy density to rest mass energy density, we found the following formula for α, the ratio of kinetic energy density to pressure

$$\alpha = \frac{6}{1 - \delta + \sqrt{\delta^2 + 6\delta + 1}} \; ; \; \delta \equiv \frac{1}{\beta}$$

The large and small β limits provide the well-known results, α = 3/2 and α = 3, respectively. The full dependence of α(β) is shown in fig. S5.

SUPPLEMENTARY MATERIALS

Supplementary material for this article is available at http://advances.sciencemag.org/cgi/content/full/3/1/e1601558/DC1

Supplementary section

fig. S1. Spectrum of an array of 55-nm-diameter Ni nanowires with an average atomic density corresponding to 30% of solid density irradiated at 4×10^{19} W cm^{-2} with an ultrahigh contrast λ = 400-nm laser pulse of 55-fs duration.

fig. S2. Computed electron density distribution in 400-nm-diameter gold nanowire irradiated at an intensity of 1×10^{22} W cm^{-2} with a 30-fs laser pulse, corresponding to the conditions in Fig. 7.

fig. S3. Electron energy distribution under the same irradiation conditions as in fig. S2 at different times with respect to the peak of the laser pulse averaged in space.

fig. S4. Computed scaling of the energy density deposited into Au nanowire arrays as a function of the irradiation intensity for two different times during the plasma evolution.

fig. S5. Ratio of kinetic energy density to pressure (α) as a function of the ratio of kinetic energy density to rest mass energy density (β).

table S1. Pressures calculated from the kinetic energy density computed by the PIC simulations using the approximation by Ryu *et al.* (*26*).

REFERENCES AND NOTES

1. S. H. Glenzer, B. J. MacGowan, P. Michel, N. B. Meezan, L. J. Suter, S. N. Dixit, J. L. Kline, G. A. Kyrala, D. K. Bradley, D. A. Callahan, E. L. Dewald, L. Divol, E. Dzenitis, M. J. Edwards, A. V. Hamza, C. A. Haynam, D. E. Hinkel, D. H. Kalantar, J. D. Kilkenny, O. L. Landen, J. D. Lindl, S. LePape, J. D. Moody, A. Nikroo, T. Parham, M. B. Schneider, R. P. J. Town, P. Wegner, K. Widmann, P. Whitman, B. K. F. Young, B. Van Wonterghem, L. J. Atherton, E. I. Moses, Symmetric inertial confinement fusion implosions at ultra-high laser energies. *Science* **327**, 1228–1231 (2010).
2. O. A. Hurricane, D. A. Callahan, D. T. Casey, P. M. Celliers, C. Cerjan, E. L. Dewald, T. R. Dittrich, T. Döppner, D. E. Hinkel, L. F. Berzak Hopkins, J. L. Kline, S. Le Pape, T. Ma, A. G. MacPhee, J. L. Milovich, A. Pak, H.-S. Park, P. K. Patel, B. A. Remington, J. D. Salmonson, P. T. Springer, R. Tommasini, Fuel gain exceeding unity in an inertially confined fusion implosion. *Nature* **506**, 343–348 (2014).
3. B. A. Remington, R. E. Rudd, J. S. Wark, From microjoules to megajoules and kilobars to gigabars: Probing matter at extreme states of deformation. *Phys. Plasmas* **22**, 090501 (2015).
4. S. Fujioka, H. Takabe, N. Yamamoto, D. Salzmann, F. Wang, H. Nishimura, Y. Li, Q. Dong, S. Wang, Y. Zhang, Y.-J. Rhee, Y.-W. Lee, J.-M. Han, M. Tanabe, T. Fujiwara, Y. Nakabayashi, G. Zhao, J. Zhang, K. Mima, X-ray astronomy in the laboratory with a miniature compact object produced by laser-driven implosion. *Nat. Phys.* **5**, 821–825 (2009).
5. B. A. Remington, D. Arnett, R. P. Drake, H. Takabe, Modeling astrophysical phenomena in the laboratory with intense lasers. *Science* **284**, 1488–1494 (1999).
6. A. B. Sefkow, G. R. Bennett, M. Geissel, M. Schollmeier, B. C. Franke, B. W. Atherton, Efficiency enhancement for K_α X-ray yields from laser-driven relativistic electrons in solids. *Phys. Rev. Lett.* **106**, 235002 (2011).
7. Y. Kitagawa, Y. Mori, O. Komeda, K. Ishii, R. Hanayama, K. Fujita, S. Okihara, T. Sekine, N. Satoh, T. Kurita, M. Takagi, T. Watari, T. Kawashima, H. Kan, Y. Nishimura, A. Sunahara, Y. Sentoku, N. Nakamura, T. Kondo, M. Fujine, H. Azuma, T. Motohiro, T. Hioki, M. Kakeno, E. Miura, Y. Arikawa, T. Nagai, Y. Abe, S. Ozaki, A. Noda, Direct heating of a laser-imploded core by ultraintense laser-driven ions. *Phys. Rev. Lett.* **114**, 195002 (2015).
8. R. Nora, W. Theobald, R. Betti, F. J. Marshall, D. T. Michel, W. Seka, B. Yaakobi, M. Lafon, C. Stoeckl, J. Delettrez, A. A. Solodov, A. Casner, C. Reverdin, X. Ribeyre, A. Vallet, J. Peebles, F. N. Beg, M. S. Wei, Gigabar spherical shock generation on the OMEGA laser. *Phys. Rev. Lett.* **114**, 045001 (2015).
9. T. R. Dittrich, O. A. Hurricane, D. A. Callahan, E. L. Dewald, T. Döppner, D. E. Hinkel, L. F. Berzak Hopkins, S. Le Pape, T. Ma, J. L. Milovich, J. C. Moreno, P. K. Patel, H.-S. Park, B. A. Remington, J. D. Salmonson, J. L. Kline, Design of a high-foot high-adiabat ICF capsule for the National Ignition Facility. *Phys. Rev. Lett.* **112**, 055002 (2014).

Downloaded from http://advances.sciencemag.org/ on January 12, 2017

10. D. J. Hoarty, P. Allan, S. F. James, C. R. D. Brown, L. M. R. Hobbs, M. P. Hill, J. W. O. Harris, J. Morton, M. G. Brookes, R. Shepherd, J. Dunn, H. Chen, E. Von Marley, P. Beiersdorfer, H. K. Chung, R. W. Lee, G. Brown, J. Emig, Observations of the effect of ionization-potential depression in hot dense plasma. *Phys. Rev. Lett.* **110**, 265003 (2013).
11. P. M. Nilson, W. Theobald, J. F. Myatt, C. Stoeckl, M. Storm, J. D. Zuegel, R. Betti, D. D. Meyerhofer, T. C. Sangster, Bulk heating of solid-density plasmas during high-intensity-laser plasma interactions. *Phys. Rev. E Stat. Nonlinear Soft Matter Phys.* **79**, 016406 (2009).
12. D. J. Hoarty, S. F. James, C. R. D. Brown, B. M. Williams, H. K. Chung, J. W. O. Harris, L. Upcraft, B. J. B. Crowley, C. C. Smith, R. W. Lee, Measurements of emission spectra from hot, dense germanium plasma in short pulse laser experiments. *High Energy Density Phys.* **6**, 105–108 (2010).
13. C. R. D. Brown, D. J. Hoarty, S. F. James, D. Swatton, S. J. Hughes, J. W. Morton, T. M. Guymer, M. P. Hill, D. A. Chapman, J. E. Andrew, A. J. Comley, R. Shepherd, J. Dunn, H. Chen, M. Schneider, G. Brown, P. Beiersdorfer, J. Emig, Measurements of electron transport in foils irradiated with a picosecond time scale laser pulse. *Phys. Rev. Lett.* **106**, 185003 (2011).
14. V. Dervieux, B. Loupias, S. Baton, L. Lecherbourg, K. Glize, C. Rousseaux, C. Reverdin, L. Gremillet, C. Blancard, V. Silvert, J.-C. Pain, C. R. D. Brown, P. Allan, M. P. Hill, D. J. Hoarty, P. Renaudin, Characterization of near-LTE, high-temperature and high-density aluminum plasmas produced by ultra-high intensity lasers. *High Energy Density Phys.* **16**, 12–17 (2015).
15. K. U. Akli, S. B. Hansen, A. J. Kemp, R. R. Freeman, F. N. Beg, D. C. Clark, S. D. Chen, D. Hey, S. P. Hatchett, K. Highbarger, E. Giraldez, J. S. Green, G. Gregori, K. L. Lancaster, T. Ma, A. J. MacKinnon, P. Norreys, N. Patel, J. Pasley, C. Shearer, R. B. Stephens, C. Stoeckl, M. Storm, W. Theobald, L. D. Van Woerkom, R. Weber, M. H. Key, Laser heating of solid matter by light-pressure-driven shocks at ultrarelativistic intensities. *Phys. Rev. Lett.* **100**, 165002 (2008).
16. F. Y. Khattak, R. J. Clarke, E. J. Divall, M. Edwards, P. S. Foster, C. J. Hooker, A. J. Langley, P. Mistry, D. Neely, O. A. M. B. Percie du Sert, J. Smith, C. Spindloe, G. Tallents, M. Tolley, D. Riley, Enhanced He-α emission from "smoked" Ti targets irradiated with 400 nm, 45 fs laser pulses. *EPL* **72**, 242–248 (2005).
17. H. A. Sumeruk, S. Kneip, D. R. Symes, I. V. Churina, A. V. Belolipetski, T. D. Donnelly, T. Ditmire, Control of strong-laser-field coupling to electrons in solid targets with wavelength-scale spheres. *Phys. Rev. Lett.* **98**, 045001 (2007).
18. M. M. Murnane, H. C. Kapteyn, S. P. Gordon, J. Bokor, E. N. Glytsis, R. W. Falcone, Efficient coupling of high-intensity subpicosecond laser pulses into solids. *Appl. Phys. Lett.* **62**, 1068 (1993).
19. S. P. Gordon, T. Donnelly, A. Sullivan, H. Hamster, R. W. Falcone, X-rays from microstructured targets heated by femtosecond lasers. *Opt. Lett.* **19**, 484–486 (1994).
20. G. Kulcsár, D. AlMawlawi, F. W. Budnik, P. R. Herman, M. Moskovits, L. Zhao, R. S. Marjoribanks, Intense picosecond x-ray pulses from laser plasmas by use of nanostructured "velvet" targets. *Phys. Rev. Lett.* **84**, 5149–5152 (2000).
21. P. P. Rajeev, P. Taneja, P. Ayyub, A. S. Sandhu, G. R. Kumar, Metal nanoplasmas as bright sources of hard X-ray pulses. *Phys. Rev. Lett.* **90**, 115002 (2003).
22. S. Mondal, I. Chakraborty, S. Ahmad, D. Carvalho, P. Singh, A. D. Lad, V. Narayanan, P. Ayyub, G. R. Kumar, J. Zheng, Z. M. Sheng, Highly enhanced hard x-ray emission from oriented metal nanorod arrays excited by intense femtosecond laser pulses. *Phys. Rev. B* **83**, 035408 (2011).
23. T. Nishikawa, S. Suzuki, Y. Watanabe, O. Zhou, H. Nakano, Efficient water-window X-ray pulse generation from femtosecond-laser-produced plasma by using a carbon nanotube target. *Appl. Phys. B* **78**, 885–890 (2004).
24. M. A. Purvis, V. N. Shlyaptsev, R. Hollinger, C. Bargsten, A. Pukhov, A. Prieto, Y. Wang, B. M. Luther, L. Yin, S. Wang, J. J. Rocca, Relativistic plasma nanophotonics for ultrahigh energy density physics. *Nat. Photonics* **7**, 796–800 (2013).
25. A. P. Shevelko, X-ray spectroscopy of laser-produced plasmas using a von Hamos spectrograph. *Proc. SPIE* **3406**, 91–108 (1998).
26. D. Ryu, I. Chattopadhyay, E. Choi, Equation of state in numerical relativistic hydrodynamics. *Astrophys. J. Suppl. Ser.* **166**, 410–420 (2006).
27. V. Kaymak, A. Pukhov, V. N. Shlyaptsev, J. J. Rocca, Nanoscale ultradense Z-pinch formation from laser-irradiated nanowire arrays. *Phys. Rev. Lett.* **117**, 035004 (2016).
28. D. S. Clark, C. R. Weber, J. L. Milovich, J. D. Salmonson, A. L. Kritcher, S. W. Haan, B. A. Hammel, D. E. Hinkel, O. A. Hurricane, O. S. Jones, M. M. Marinak, P. K. Patel, H. F. Robey, S. M. Sepke, M. J. Edwards, Three-dimensional simulations of low foot and high foot implosion experiments on the National Ignition Facility. *Phys. Plasmas* **23**, 056302 (2016).
29. T. Ditmire, J. Zweiback, V. P. Yanovsky, T. E. Cowan, G. Hays, K. B. Wharton, Nuclear fusion from explosions of femtosecond laser-heated deuterium clusters. *Nature* **398**, 489–492 (1999).
30. J. P. Hoare, On the role of boric-acid in the Watts bath. *J. Electrochem. Soc.* **133**, 2491–2494 (1986).
31. A. Pukhov, Three-dimensional electromagnetic relativistic particle-in-cell code VLPL (Virtual Laser Plasma Lab). *J. Plasma Phys.* **61**, 425–433 (1999).
32. A. Zhidkov, A. Sasaki, Effect of field ionization on interaction of an intense subpicosecond laser pulse with foils. *Phys. Plasmas* **7**, 1341–1344 (2000).
33. A. Karmakar, A. Pukhov, Collimated attosecond GeV electron bunches from ionization of high-Z material by radially polarized ultra-relativistic laser pulses. *Laser Part. Beams* **25**, 371–377 (2007).
34. V. N. Shlyaptsev, J. J. G. Rocca, A. L. Osterheld, Dynamics of a capillary discharge x-ray laser. *Proc. SPIE* **2520**, 365–372 (1995).
35. M. Klapisch, M. Busquet, A. Bar-Shalom, A new and improved version of HULLAC. *AIP Conf. Proc.* **926**, 206 (2007).
36. L. M. Biberman, V. S. Vorob'ev, I. T Yakubov, *Kinetics of Nonequilibrium Low-Temperature Plasmas* (Springer, 1987), 498 pp.
37. T. Holstein, Imprisonment of resonance radiation in gases. *Phys. Rev.* **72**, 1212–1233 (1947).
38. J. L. Synge, *The Relativistic Gas* (North-Holland Publishing Co., 1957).

Acknowledgments: We acknowledge M. Purvis for helpful discussions. **Funding:** This work was funded by the High Energy Density Laboratory Plasmas program, Fusion Energy Sciences, Office of Science of the U.S. Department of Energy (grant DE-SC0014610), and a previous grant from the Defense Threat Reduction Agency (grant HDTRA-1-10-1-0079). The work of Lawrence Livermore National Laboratory researchers was performed under the auspices of the U.S. Department of Energy under contract no. DE-AC52-07NA27344. **Author contributions:** The concept of the experiment was proposed by J.J.R., and the experiment was designed by J.J.R., C.B., and R.H. Modeling was performed by V.N.S., V.K., A.P., and R.L. using atomic data computed by M.B. and M.K. The targets were developed and manufactured by C.B., M.G.C., and D.K. The experiments and related measurements were conducted by C.B., R.H., S.W., A.R., Y.W., R.T., J.P., and J.J.R. All authors participated in the writing of the manuscript. **Competing interests:** The authors declare that they have no competing interests. **Data and materials availability:** All data needed to evaluate the conclusions in the paper are present in the paper and/or the Supplementary Materials. Additional data related to this paper may be requested from the authors.

Submitted 7 July 2016
Accepted 28 November 2016
Published 11 January 2017
10.1126/sciadv.1601558

Citation: C. Bargsten, R. Hollinger, M. G. Capeluto, V. Kaymak, A. Pukhov, S. Wang, A. Rockwood, Y. Wang, D. Keiss, R. Tommasini, R. London, J. Park, M. Busquet, M. Klapisch, V. N. Shlyaptsev, J. J. Rocca, Energy penetration into arrays of aligned nanowires irradiated with relativistic intensities: Scaling to terabar pressures. *Sci. Adv.* **3**, e1601558 (2017).

Downloaded from http://advances.sciencemag.org/ on January 12, 2017

Science Advances

Energy penetration into arrays of aligned nanowires irradiated with relativistic intensities: Scaling to terabar pressures

Clayton Bargsten, Reed Hollinger, Maria Gabriela Capeluto, Vural Kaymak, Alexander Pukhov, Shoujun Wang, Alex Rockwood, Yong Wang, David Keiss, Riccardo Tommasini, Richard London, Jaebum Park, Michel Busquet, Marcel Klapisch, Vyacheslav N. Shlyaptsev and Jorge J. Rocca (January 11, 2017)

Sci Adv 2017, 3:.
doi: 10.1126/sciadv.1601558

This article is publisher under a Creative Commons license. The specific license under which this article is published is noted on the first page.

For articles published under CC BY licenses, you may freely distribute, adapt, or reuse the article, including for commercial purposes, provided you give proper attribution.

For articles published under CC BY-NC licenses, you may distribute, adapt, or reuse the article for non-commerical purposes. Commercial use requires prior permission from the American Association for the Advancement of Science (AAAS). You may request permission by clicking here.

The following resources related to this article are available online at http://advances.sciencemag.org. (This information is current as of January 12, 2017):

Updated information and services, including high-resolution figures, can be found in the online version of this article at:
http://advances.sciencemag.org/content/3/1/e1601558.full

Supporting Online Material can be found at:
http://advances.sciencemag.org/content/suppl/2017/01/09/3.1.e1601558.DC1

This article **cites 36 articles,** 3 of which you can access for free at:
http://advances.sciencemag.org/content/3/1/e1601558#BIBL

Science Advances (ISSN 2375-2548) publishes new articles weekly. The journal is published by the American Association for the Advancement of Science (AAAS), 1200 New York Avenue NW, Washington, DC 20005. Copyright is held by the Authors unless stated otherwise. AAAS is the exclusive licensee. The title Science Advances is a registered trademark of AAAS

Downloaded from http://advances.sciencemag.org/ on January 12, 2017

Research Article Vol. 4, No. 11 / November 2017 / Optica 1344

optica

Efficient picosecond x-ray pulse generation from plasmas in the radiation dominated regime

Reed Hollinger,[1,6] Clayton Bargsten,[1] Vyacheslav N. Shlyaptsev,[1] Vural Kaymak,[4] Alexander Pukhov,[4] Maria Gabriela Capeluto,[5] Shoujun Wang,[1] Alex Rockwood,[2] Yong Wang,[1] Amanda Townsend,[2] Amy Prieto,[3] Patrick Stockton,[1] Alden Curtis,[1] and Jorge J. Rocca[1,2,*]

[1]Electrical and Computer Engineering Department, Colorado State University, Fort Collins, Colorado 80523, USA
[2]Physics Department, Colorado State University, Fort Collins, Colorado 80523, USA
[3]Chemistry Department, Colorado State University, Fort Collins, Colorado 80523, USA
[4]Institut für Theoretische Physik 1, Heinrich-Heine-Universität Düsseldorf, 40225 Düsseldorf, Germany
[5]Departamento de Física, FCEyN, UBA and IFIBA, CONICET, Pabellón 1, Ciudad Universitaria, 1428 Buenos Aires, Argentina
[6]e-mail: reed.hollinger@colostate.edu
*Corresponding author: jorge.rocca@colostate.edu

Received 24 July 2017; revised 29 September 2017; accepted 2 October 2017 (Doc. ID 303129); published 27 October 2017

The efficient conversion of optical laser light into bright ultrafast x-ray pulses in laser created plasmas is of high interest for dense plasma physics studies, material science, and other fields. However, the rapid hydrodynamic expansion that cools hot plasmas has limited the x-ray conversion efficiency (CE) to 1% or less. Here we demonstrate more than one order of magnitude increase in picosecond x-ray CE by tailoring near solid density plasmas to achieve a large radiative to hydrodynamic energy loss rate ratio, leading into a radiation loss dominated plasma regime. A record 20% CE into $h\nu > 1$ keV photons was measured in arrays of large aspect ratio Au nanowires heated to keV temperatures with ultrahigh contrast femtosecond laser pulses of relativistic intensity. The potential of these bright ultrafast x-ray point sources for table-top imaging is illustrated with single shot flash radiographs obtained using low laser pulse energy. These results will enable the deployment of brighter laser driven x-ray sources at both compact and large laser facilities. © 2017 Optical Society of America

OCIS codes: (040.7480) X-rays, soft x-rays, extreme ultraviolet (EUV); (320.7090) Ultrafast lasers; (110.7440) X-ray imaging; (350.5400) Plasmas; (160.4236) Nanomaterials.

https://doi.org/10.1364/OPTICA.4.001344

1. INTRODUCTION

Intense ultrashort bursts of x-ray radiation are essential for backlighting the implosion of capsules in inertial confinement fusion experiments [1,2]. They are also of significant interest for fundamental studies that include laboratory opacity measurements in matter at the conditions of stellar interiors [3], and for probing ultrafast changes in material with high spatial and temporal resolution [4,5]. Dense plasmas produced by laser irradiation of solid density materials with intense femtosecond laser pulses are emitters of intense x-ray pulses. However, different factors contribute to limit the CE into ultrafast x-ray pulses. First, only a fraction of the laser energy is absorbed by the plasma. Second, the radiation typically originates from a shallow plasma volume whose rapid expansion results in hydrodynamic cooling rates that exceed the radiation cooling rate. The result is poor conversion efficiency. Efforts to increase the ultrafast x-ray yield have largely focused on addressing the first of these two limitations by improving the coupling of the laser energy into the material using structured targets. Targets investigated include micro-lithographic gratings [6–8], nanometer-size dielectric spheres or ellipsoids [9,10], "smoked" clustered surfaces [7,11,12], and nanowire arrays [12–16]. Increased CE with respect to flat solid targets has been reported [6,11,12,14–17]. In the case of nanowires, the increased x-ray yield was often adjudicated to increased absorption [12,14], including enhanced absorption due to a "lightning rod effect" that increases the number of hot electrons as a result of an enhancement of the electric field at the tip of nanostructures [15,17]. In addition to increased absorption, Kulcsar *et al.* suggested other causes that include a larger number of heated atoms [12]. However, the CE into $h\nu > 0.9$ keV x-rays was limited to ~0.1%, a value similar to that obtained using smoke targets. In all the experiments with different types of nanostructured targets, the x-ray CE into $h\nu > 1$ keV photons has remained less than 1%, in spite of the increase in energy coupling. This CE into picosecond x-ray pulses is significantly lower than that achieved in converting laser light into nanosecond x-ray pulses in underdense gas or cavity and pre-exploded foil plasmas [18–22].

In this paper, we show that an increase of more than one order of magnitude in optical to picosecond x-ray CE can be achieved by tailoring the plasma characteristics to reach a smaller radiative

cooling time, τ_{rad}, than the hydrodynamic cooling time, τ_{hydro}, resulting in a larger radiative to hydrodynamic cooling rate ratio that effectively overcomes hydrodynamic cooling. The radiative cooling time is defined here as the time needed to radiatively dissipate the thermal energy of the plasma. In the simple case of an ideal plasma with ions of average charge Z, this characteristic time can be expressed as the ratio of the kinetic energy of free electrons to their rate of radiated energy loss by collisions: $\frac{3ZkT_e}{2E}\frac{1}{\langle\sigma v\rangle n_e}$, where σ is the effective electron collision cross section for all three major radiative processes (line radiation, photorecombination, and bremsstrahlung), T_e and n_e are the electron temperature and density, respectively, and E is the average energy radiated per collision event. The hydrodynamic cooling time is defined here as $\Delta L/C_s$, where ΔL is plasma size and C_s is the acoustic velocity. Considering that, within the range of high electron densities and high temperatures of interest for x-ray generation, τ_{rad} is inversely proportional to the electron-density-dependent total collision rate $\langle\sigma v\rangle n_e$ and τ_{hydro} is proportional to the plasma size ΔL, this condition requires a large electron density and/or large plasma size such that

$$\tau_{\mathrm{rad}} \propto \frac{1}{\langle\sigma v\rangle n_e} < \frac{\Delta L}{C_s} \propto \tau_{\mathrm{hydro}}. \tag{1}$$

We experimentally demonstrate that this approach results in an ~20% CE of optical laser light into $h\nu > 1$ keV x-rays in 4π sr, more than one order of magnitude increase in CE with respect to previous work. We fulfilled the inequality in Eq. (1) by volumetrically heating supercritical density plasmas by irradiating arrays of high aspect ratio Au or Ni nanowires at an intensity of $I \sim 4 \times 10^{19}$ W cm^{-2} with ultrahigh contrast femtosecond laser pulses. The interaction was tailored to simultaneously achieve deep volumetric heating (large ΔL) to multi-keV temperatures, and plasma densities of the order of 100 times the critical density in which the collisional rates are greatly increased with respect to plasmas generated from solid targets.

2. METHODS

The experiments were conducted by irradiating arrays of free-standing, vertically aligned Au and Ni nanowires with diameters of 55, 80, or 100 nm and 4–6 μm in length. The laser beam impinged parallel to the nanowire axis, normal to the nanowire array target surface. The nanowire arrays were synthesized by electrodeposition into anodic aluminum oxide templates [23]. The nanowires were grown with an average density of 12% solid density for the targets composed of 55 or 80 nm diameter nanowires, and 15% of solid density for the 100 nm diameter nanowire targets. After dissolving the template, an array of ordered, high aspect ratio (~50–100∶1) nanowires is exposed. This corresponds to an interwire spacing of 85 and 130 nm for the 55 and 100 nm diameter wire arrays, respectively. Each nanowire target was imaged using a scanning electron microscope. The nanostructured targets were irradiated by ultrahigh ($>10^{12}$) contrast $\lambda = 400$ nm pulses of ~55 fs duration with energy up to 1 J from a frequency-doubled Ti:sapphire chirped-pulse-amplification (CPA) laser. The laser consists of a conventional front end followed by three Ti:sapphire power amplifiers pumped by Nd:glass slab lasers designed to operate at up to 5 Hz repetition rate [24]. The beam was expanded to 9 cm, and the pulses were compressed using a gold grating vacuum compressor. Frequency doubling in a 0.8 mm thick Type I KDP crystal with an efficiency of 40%–50% greatly improves the contrast, as the second-harmonic generation process is proportional to the square of the intensity. The duration of the frequency-doubled pulse was measured in a single shot self-diffraction autocorrelator. The wavefront was corrected with a deformable mirror (Imagine Optic). The high contrast pulses were focused onto the target by a 90 deg off-axis parabolic mirror with a 15.4 cm focal length, resulting in a spot size of ~4.5 μm to obtain an intensity of $\sim 4 \times 10^{19}$ W cm^{-2}.

The angular distribution of the x-ray emission was measured using an array of four filtered Si photodiodes mounted at equally spaced polar angles on a 28 cm radius circular rail centered on the laser beam focus where the target was placed. Polished Ni or Au flat solid targets were shot immediately preceding each nanowire target shot for comparison. The diodes were placed on a plane that forms an angle of 20 deg with respect to the plane of incidence. Magnet pairs were placed in the front of each of the photodiodes to deflect electrons up to 6 MeV energy away from the diodes. It was verified that increasing the magnetic field strength by 2 × and the length of the magnets by the same factor did not change the photodiode signals, ensuring that the photodiode/filter assembly is in practice only detecting x-rays. The spectrally resolved x-ray emission was simultaneously recorded using a von Hamos mica crystal spectrometer and a front illuminated CCD. Time integrated spectral emission of the plasmas showed He-like Ni ion lines that dominate over the characteristic K-α emission by over one order of magnitude.

3. RESULTS AND DISCUSSION

Figure 1 illustrates a particle-in-cell simulation (PIC) of the electron temperature and electron density evolution in an array of Au nanowires at three different times after the laser pulse. The array is composed of wires 55 nm in diameter with an average density corresponding to 12% of solid density, and the laser pulse has a 55 fs FWHM duration. The simulation was conducted using the fully relativistic 3-D PIC code Virtual Laser-Plasma Laboratory (VLPL) [25]. In contrast to flat solid targets, where a thin plasma layer is heated, in nanowire arrays the ultrafast laser pulses propagate several micrometers within the interwire gaps. The heated nanowires explode, creating a thick plasma layer of nearly solid density, reaching $n_e \sim 4 \times 10^{23}$ cm^{-3} 311 fs after the peak of the laser pulse, while the electron temperature is ~15 keV [Figs. 1(c) and 1(f)]. Later the plasma cools, but 1 ps after the peak of the laser pulse the temperature still remains at a few keV. To illustrate the major radiative differences between a flat solid target and a volumetrically heated nanowire array, Fig. 2 shows the computed x-ray radiation power density spatial distribution as a function of time up to 10 ps after the laser pulse. The simulations are the result of hydrodynamic model computations with transient atomic kinetics in which the VLPL PIC code was used to simulate the first stages of nanowire plasma formation until the nanowires are fully dissolved. Both targets are assumed to be irradiated with an intensity of 4×10^{19} W cm^{-2}. It is shown that irradiation of the Au nanowire array results in both a large increase in the radiating volume and a larger emitted power density. In the case of the flat solid target, most of the x-ray emission takes place in a very thin supercritical layer heated by conduction, where acceleration and expansion cooling take place, with the plasma density rapidly dropping orders of magnitude in

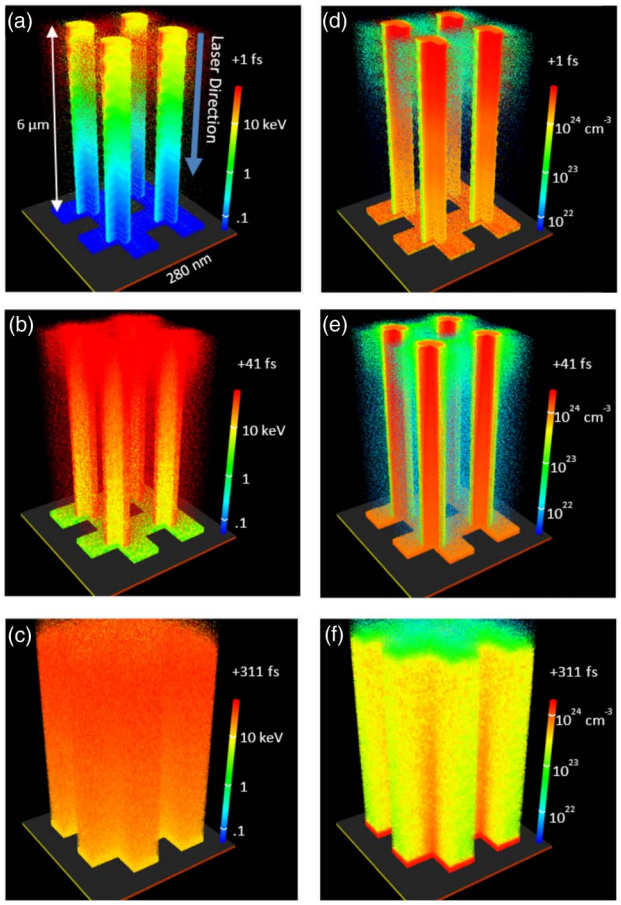

Fig. 1. (a)–(c) PIC simulation of the electron temperature distribution in a 55 nm diameter Au nanowire array irradiated by a $\lambda = 400$ nm laser pulse of 55 fs duration at an intensity of 4×10^{19} W cm^{-2} at three different times after the laser pulse. (d)–(f) show the corresponding electron density maps.

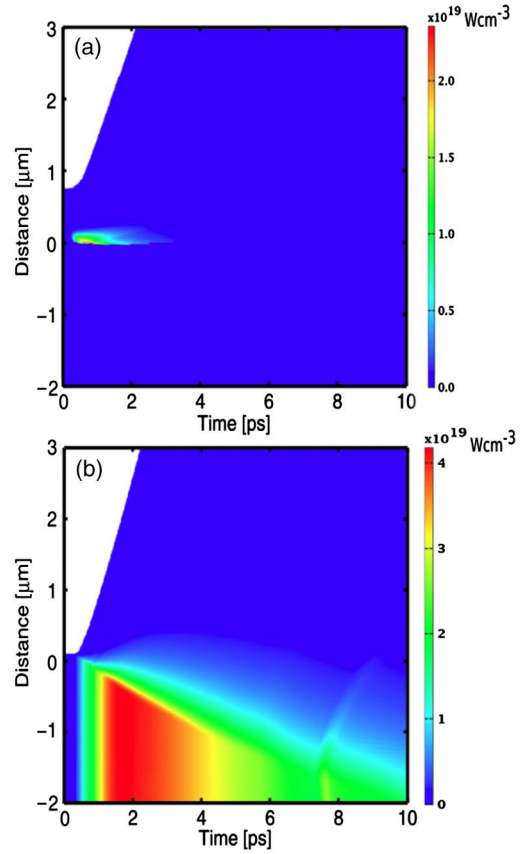

Fig. 2. Computed evolution of the x-ray radiation power for (a) a Au flat target and (b) a Au nanowire target, both irradiated at an intensity of 4×10^{19} W cm^{-2} with a 55 fs FWHM pulse. The array of nanowires is assumed to be composed of 55 nm diameter wires with an average density of 12% solid. Time is measured with respect to the peak of the laser pulse, and the distance is in the direction normal to the target surface.

1 mm. The much larger heated plasma depth in the nanowire plasma greatly increases the plasma hydrodynamic cooling time. Simultaneously, the larger plasma density results in an increased electron collisional excitation rate, leading to a shorter radiative cooling time.

The magnitude of these effects is quantitatively illustrated in Fig. 3 by atomic kinetic calculations that compare the characteristic radiative and hydrodynamic cooling times of a Au flat target plasma and a Au nanowire array plasma. The computations were conducted with the hydrodynamic/atomic physics code Radex [26]. Figure 3(a) shows the cooling times for Au plasma with a density of $n_e = 6 \times 10^{22}$ cm^{-3} and a thickness of 0.2 µm. These are the typical parameters of the x-ray emitting layer computed by both PIC and hydrodynamic models for plasmas created by irradiating a solid Au target. Both models give similar source thickness values in spite of the fact that RADEX is approaching the validity limit of the hydrodynamic approximation. In this case, the great majority of the laser energy is lost in the hydrodynamic expansion before collisions have time to convert the electron kinetic energy into radiation. For the electron temperatures of interest, the hydrodynamic cooling time is much shorter than the radiative cooling time, resulting in a small CE. This result is in contrast to Fig. 3(b) for a supercritical Au plasma with a density of $n_e = 4 \times 10^{23}$ cm^{-3}, a value approaching 100 times the critical density, typical of the conditions resulting from irradiating the nanowire arrays with the intensity we used in the experiments. In this case the radiative cooling time is smaller than the hydrodynamic cooling time, leading to greatly increased radiation efficiency.

For larger average density nanowire arrays irradiated at increased intensities, even higher electron densities will result [27], further driving the plasma into a radiation loss dominated regime.

The large increase in CE we report here is made possible by selecting a combination of irradiation and target parameters designed to achieve the condition in Eq. (1). First, we use ultrahigh contrast $>10^{12}$ laser pulses that avoid destroying the nanowires and establishing a critical density layer before the main pulse arrives. Second, we use short laser pulses (55 fs) that allow for nearly all of the laser energy to be deposited deep into the array before the nanowires explode and close the interwire gap, forming a continuous critical density surface. After this time, no further efficient coupling of the laser energy can occur into the volumetrically heated plasma. Third, the use of long nanowires allows for volumetric heating to occur to depths of 4–5 µm [27], increasing the hydrodynamic expansion time. Fourth, we use dense arrays, in which the plasma density reaches nearly 100 times the critical

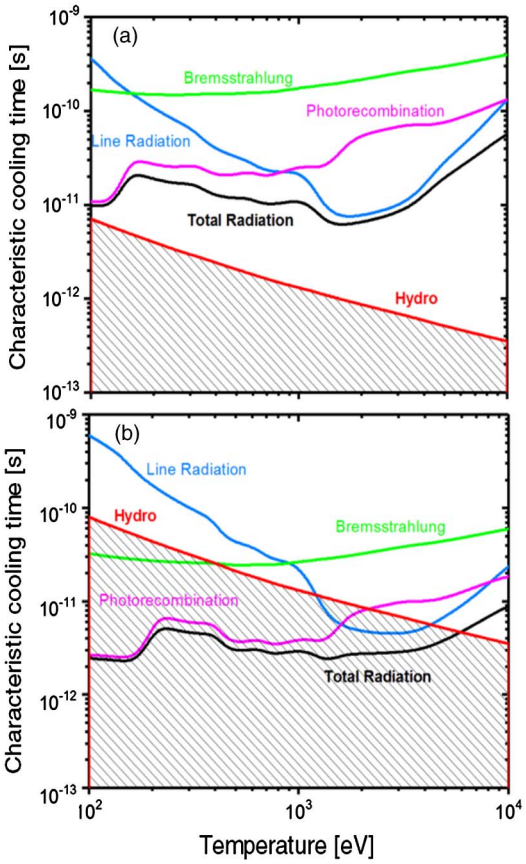

Fig. 3. Comparison of radiative and hydrodynamic cooling times as a function of electron temperature for two different Au plasmas with characteristics corresponding to the x-ray emitting region of (a) a flat solid target, $n_e = 6 \times 10^{22}$ cm^{-3}, plasma size $L = 0.2$ μm, and (b) a nanowire array plasma $n_e = 4 \times 10^{23}$ cm^{-3} and plasma size $L = 4$ μm. The total radiation time is the effective radiative cooling time computed from the photorecombination, bremsstrahlung, and line radiation rates.

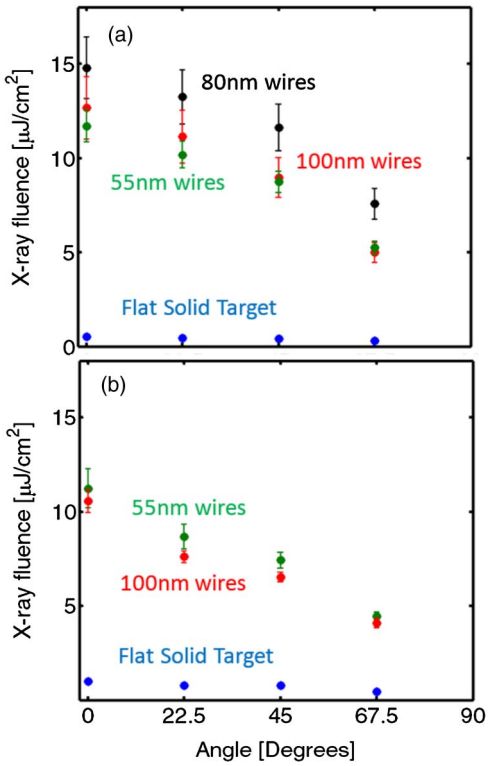

Fig. 4. Measured angular distribution of the x-ray fluence on each diode from nanowire arrays at photon energies >1 keV for (a) Au and (b) Ni nanowire targets of different nanowire diameters. Measurements for flat solid targets of the same materials are included for comparison. The irradiation intensity was 4×10^{19} W cm^{-2}. Error bars correspond to 1 standard deviation. Fluctuations in x-ray CE result mostly from irregularities and imperfections in the ordered wire array. The angle is measured with respect to the normal to the target surface.

density, which results in high collisional rates and, consequently, in very short radiative cooling times. Fifth, we use relativistic irradiation intensities that heat the plasmas to multi-keV temperatures deep into the array, which leads to a high degree of ionization [16], an increased electron density, and a decreased radiation lifetime. This simultaneous set of conditions differs from those in previous experiments that measured x-ray yield from nanowire targets. Prior work used either picosecond pulses [12], short wires [12,14], relatively low contrast pulses [12–14], or non-relativistic intensities [11–14]. This limited the radiation fraction obtained for $h\nu > 1$ keV to values nearly two orders of magnitude smaller than that we report here.

For photon energies $h\nu > 1$ keV, both Au and Ni nanowires display a convex angular emission profile with maximum intensity in the direction normal to the target (Fig. 4), resulting from increased opacity in the periphery of the plasma. Integration of these emission profiles over a hemisphere gives us the total x-ray yields shown in Fig. 5. Comparison of the x-ray CE for Au and Ni nanowire array targets of different wire diameters shows that the x-ray emission is higher for Au. CE is defined here as the ratio of the measured x-ray energy for photons $h\nu > 1$ keV (or >6 keV) emitted into 4π sr divided by the laser drive energy impinging onto the target. The highest yield corresponds to targets with 80 nm diameter Au nanowires, with an average CE of 18% and individual shots reaching values up to 22% in 4π sr [Fig. 5(a)]. This CE for $h\nu > 1$ keV exceeds the highest reported values reported using any type of target by more than one order of magnitude [6] and those reported for nanowire targets by two orders of magnitude [12]. Figure 5(b) compares the $h\nu > 6$ keV plasma emission from Au nanowire targets of different nanowire diameters to that from a Au foil target irradiated with the same pulses. At these energies, the active region of the Si detector starts to become transparent to the radiation. We corrected the measured photodiode signal for the 50 μm thickness of the Si detector active region, and also for the energy dependency of the filter transmissivity. For the latter, since model simulations show there is no line radiation above 6 keV for these transient Au plasmas, we assumed the spectral distribution is that resulting from bremsstrahlung plus photorecombination. This continuum radiation was calculated using the electron energy distribution computed by PIC simulations. With these corrections, the 80 nm Au nanowire targets are estimated to radiate at $h\nu > 6$ keV with a CE that exceed 0.8% in 4π sr, an increase of 14 times over Au foils irradiated by the same laser pulses.

The increase in x-ray flux, the small source size of ~5 μm deduced from the penumbra in a knife edge test, and the picosecond pulse duration makes these plasmas an excellent x-ray point source for time-resolved flash radiography. To illustrate this,

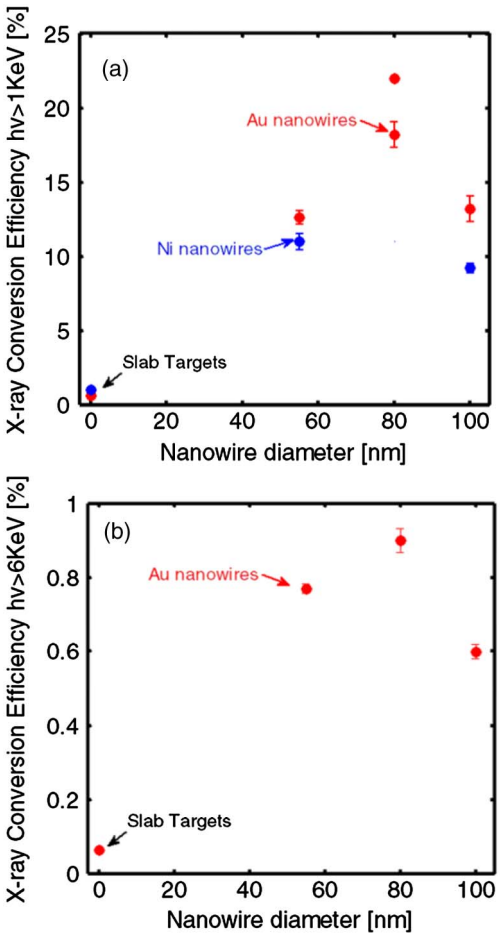

Fig. 5. (a) x-ray CE ($h\nu > 1$ keV) for Au and Ni nanowire arrays of different wire diameters compared to flat solid targets of the same material. $I = 4 \times 10^{19}$ W cm^{-2}. The values are averages of 10 shots. Error bars correspond to 1 standard deviation. The maximum measured single shot CE for 80 nm diameter wires exceeded 22% in 4π sr, which is represented by the point without an error bar. This yield corresponds to an increase of 35 × with respect to a polished flat target; (b) CE into $h\nu > 6$ keV x-rays. An enhancement of 14 × in x-ray emission is observed compared to flat targets.

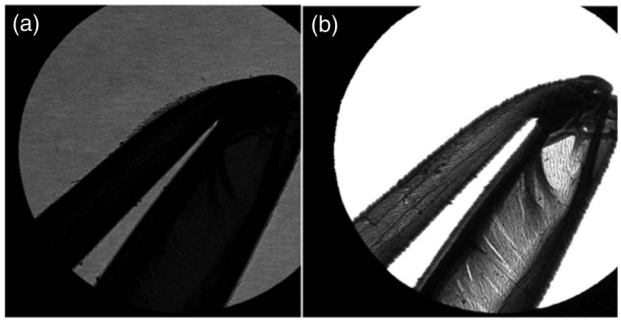

Fig. 6. Single shot radiograph of a wasp's knee using the x-ray flash emitted from (a) a flat Ni target, and (b) an array of 100 nm Ni nanowires. A 13 μm Be filter was used to block photons of $h\nu < 1$ keV. The sample was placed at 4 cm from the plasma, and a CCD array was placed at a distance of 35 cm from the sample, leading to an effective magnification of 8.75 × with a field of view of 425 μm. Both images are plotted on the same intensity scale. The laser energy on target was 25 mJ.

we conducted a single shot radiography experiment of a wasp's knee. Figure 6(b) compares a single shot radiograph taken by irradiating an array of 100 nm diameter Ni nanowires with 15% solid density to that obtained by irradiating a flat Ni solid target with a similar laser pulse [Fig. 6(a)]. The radiograph taken with the nanowire target shows that a single laser shot with a laser pulse energy of only 25 mJ on target is sufficient to produce a detailed image. In comparison, the image obtained with the flat Ni target shows insufficient flux and would require over one order of magnitude more shots to obtain a similar image.

4. CONCLUSIONS

In conclusion, we have demonstrated that the CE of optical laser pulses into picosecond x-ray pulses can be greatly improved by increasing the radiative to hydrodynamic energy loss rate ratio in volumetrically heated supercritical density plasmas. By tailoring nanostructured targets irradiated at relativistic intensities to fulfill this condition, we have generated ultrafast pulses of $h\nu > 1$ keV photons with a record efficiency of ∼20% into 4π sr. This increase of more than one order of magnitude in the efficient generation of picosecond line and continuum x-ray radiation will open new opportunities in flash radiography, including the backlighting of imploding capsules in laser fusion experiments, in opacity measurements of matter at the conditions of stellar interiors, and in table-top applications requiring intense picosecond flashes of x-rays. Furthermore, the results will also motivate more efficient x-ray generation experiments at larger laser facilities.

Funding. Fusion Sciences Program of the Office of Science (SC) of the U.S. Department of Energy (DE-SC0014610)

Acknowledgment. We acknowledge encouraging discussions with Michael Purvis and the use of the CU-CSU Summit Computer (ACI-1532235) and previous support from the Defense Threat Reduction Agency (HDTRA-1-10-1-0079).

REFERENCES

1. F. J. Marshall, P. W. McKenty, J. A. Delettrez, R. Epstein, J. P. Knauer, V. A. Smalyuk, J. A. Frenje, C. K. Li, R. D. Petrasso, F. H. Séguin, and R. C. Mancini, "Plasma-density determination from x-ray radiography of laser-driven spherical implosions," Phys. Rev. Lett. **102**, 185004 (2009).
2. C. M. Huntington, C. M. Krauland, C. C. Kuranz, R. P. Drake, H. S. Park, D. H. Kalantar, B. R. Maddox, B. A. Remington, and J. Kline, "Development of a short duration backlit pinhole for radiography on the National Ignition Facility," Rev. Sci. Instrum. **81**, 10E536 (2010).
3. J. E. Bailey, T. Nagayama, G. P. Loisel, G. A. Rochau, C. Blancard, J. Colgan, P. Cosse, G. Faussurier, C. J. Fontes, F. Gilleron, I. Golovkin, S. B. Hansen, C. A. Iglesias, D. P. Kilcrease, J. J. Macfarlane, R. C. Mancini, S. N. Nahar, C. Orban, J. Pain, A. K. Pradhan, M. Sherrill, and B. G. Wilson, "A higher-than-predicted measurement of iron opacity at solar interior temperatures," Nature **517**, 56–59 (2015).
4. B. Yaakobi, T. R. Boehly, D. D. Meyerhofer, T. J. B. Collins, B. A. Remington, P. G. Allen, S. M. Pollaine, H. E. Lorenzana, and J. H. Eggert, "EXAFS measurement of iron bcc-to-hcp phase transformation in nanosecond-laser shocks," Phys. Rev. Lett. **95**, 1–4 (2005).
5. A. Cavalleri, C. W. Siders, F. L. H. Brown, D. M. Leitner, C. Tóth, J. A. Squier, C. P. J. Barty, K. R. Wilson, K. Sokolowski-Tinten, M. Horn Von Hoegen, D. von Der Linde, and M. Kammler, "Anharmonic lattice dynamics in germanium measured with ultrafast x-ray diffraction," Phys. Rev. Lett. **85**, 586–589 (2000).
6. M. M. Murnane, H. C. Kapteyn, S. P. Gordon, J. Bokor, E. N. Glytsis, and R. W. Falcone, "Efficient coupling of high-intensity subpicosecond laser pulses into solids," Appl. Phys. Lett. **62**, 1068–1070 (1993).

7. S. P. Gordon, T. Donnelly, A. Sullivan, H. Hamster, and R. W. Falcone, "X rays from microstructured targets heated by femtosecond lasers," Opt. Lett. **19**, 484–486 (1994).
8. S. Kahaly, S. K. Yadav, W. M. Wang, S. Sengupta, Z. M. Sheng, A. Das, P. K. Kaw, and G. R. Kumar, "Near-complete absorption of intense, ultrashort laser light by sub- gratings," Phys. Rev. Lett. **101**, 145001 (2008).
9. P. P. Rajeev, P. Taneja, P. Ayyub, A. S. Sandhu, and G. R. Kumar, "Metal nanoplasmas as bright sources of hard x-ray pulses," Phys. Rev. Lett. **90**, 115002 (2003).
10. H. A. Sumeruk, S. Kneip, D. R. Symes, I. V. Churina, A. V. Belolipetski, T. D. Donnelly, and T. Ditmire, "Control of strong-laser-field coupling to electrons in solid targets with wavelength-scale spheres," Phys. Rev. Lett. **98**, 45001 (2007).
11. F. Y. Khattak, R. J. Clarke, E. J. Divall, M. Edwards, P. S. Foster, C. J. Hooker, A. J. Langley, O. A. M. B. du Sert Percie, C. Spindloe, G. Tallents, D. Riley, P. Mistry, D. Neely, J. Smith, and M. Tolley, "Enhanced He-alpha emission from "smoked" Ti targets irradiated with 400 nm, 45 fs laser pulses," Europhys. Lett. **72**, 242–248 (2005).
12. G. Kulcsar, D. AlMawlawi, F. Budnik, P. Herman, M. Moskovits, L. Zhao, and R. Marjoribanks, "Intense picosecond x-ray pulses from laser plasmas by use of nanostructured 'Velvet' targets," Phys. Rev. Lett. **84**, 5149–5152 (2000).
13. T. Nishikawa, H. Nakano, K. Oguri, N. Uesugi, M. Nakao, K. Nishio, and H. Masuda, "Nanocylinder-array structure greatly increases the soft x-ray intensity generated from femtosecond-laser-produced plasma," Appl. Phys. B **73**, 185–188 (2001).
14. A. V. Ovchinnikov, O. F. Kostenko, O. V. Chefonov, O. N. Rosmej, N. E. Andreev, M. B. Agranat, J. L. Duan, J. Liu, and V. E. Fortov, "Characteristic x-rays generation under the action of femtosecond laser pulses on nano-structured targets," Laser Part. Beams **29**, 249–254 (2011).
15. S. Mondal, I. Chakraborty, S. Ahmad, D. Carvalho, P. Singh, A. D. Lad, V. Narayanan, P. Ayyub, G. R. Kumar, J. Zheng, and Z. M. Sheng, "Highly enhanced hard x-ray emission from oriented metal nanorod arrays excited by intense femtosecond laser pulses," Phys. Rev. B **83**, 1–5 (2011).
16. M. A. Purvis, V. N. Shlyaptsev, R. Hollinger, C. Bargsten, A. Pukhov, A. Prieto, Y. Wang, B. M. Luther, L. Yin, S. Wang, and J. J. Rocca, "Relativistic plasma nanophotonics for ultrahigh energy density physics," Nat. Photonics **7**, 796–800 (2013).
17. P. P. Rajeev, P. Ayyub, S. Bagchi, and G. R. Kumar, "Nanostructures, local fields, and enhanced absorption in intense light-matter interaction," Opt. Lett. **29**, 2662–2664 (2004).
18. M. J. May, Y. P. Opachich, G. E. Kemp, J. D. Colvin, M. A. Barrios, K. W. Widmann, K. B. Fournier, M. Hohenberger, F. Albert, and S. P. Regan, "Demonstration of a long pulse x-ray source at the National Ignition Facility," Phys. Plasmas **24**, 042701 (2017).
19. F. Pérez, J. J. Kay, J. R. Patterson, J. Kane, B. Villette, F. Girard, C. Reverdin, M. May, J. Emig, C. Sorce, J. Colvin, S. Gammon, J. Jaquez, J. H. Satcher, and K. B. Fournier, "Efficient laser-induced 6–8 keV x-ray production from iron oxide aerogel and foil-lined cavity targets," Phys. Plasmas **19**, 083101 (2012).
20. E. L. Dewald, M. Rosen, S. H. Glenzer, L. J. Suter, F. Girard, J. P. Jadaud, J. Schein, C. Constantin, F. Wagon, G. Huser, P. Neumayer, and O. L. Landen, "X-ray conversion efficiency of high-Z Hohlraum wall materials for indirect drive ignition," Phys. Plasmas **15**, 072706 (2008).
21. D. Babonneau, M. Primout, F. Girard, J. P. Jadaud, M. Naudy, B. Villette, S. Depierreux, C. Blancard, G. Faussurier, K. B. Fournier, L. Suter, R. Kauffman, S. Glenzer, M. C. Miller, J. Grün, and J. Davis, "Efficient multi-keV x-ray sources from laser-exploded metallic thin foils," Phys. Plasmas **15**, 092702 (2008).
22. C. A. Back, J. Grun, C. Decker, L. J. Suter, J. Davis, O. L. Landen, R. Wallace, W. W. Hsing, J. M. Laming, U. Feldman, M. C. Miller, and C. Wuest, "Efficient multi-keV underdense laser-produced plasma radiators," Phys. Rev. Lett. **87**, 275003 (2001).
23. A. L. Prieto, M. Martín-González, J. Keyani, R. Gronsky, T. Sands, and A. M. Stacy, "The electrodeposition of high-density, ordered arrays of $Bi_{1-x}Sb_x$ nanowires," J. Am. Chem. Soc. **125**, 2388–2389 (2003).
24. D. H. Martz, D. Alessi, B. M. Luther, Y. Wang, D. Kemp, M. Berrill, and J. J. Rocca, "High-energy 13.9 nm table-top soft-x-ray laser at 2.5 Hz repetition rate excited by a slab-pumped Ti:sapphire laser," Opt. Lett. **35**, 1632–1634 (2010).
25. A. Pukhov, "Three-dimensional electromagnetic relativistic particle-in-cell code VLPL (Virtual Laser Plasma Lab)," J. Plasma Phys. **61**, 425–433 (1999).
26. A. V. Vinogradov and V. N. Shlyaptsev, "Characteristics of a laser plasma x-ray source (review)," Sov. J. Quantum Electron. **17**, 1–14 (1987).
27. C. Bargsten, R. Hollinger, M. G. Capeluto, V. Kaymak, A. Pukhov, S. Wang, A. Rockwood, Y. Wang, D. Keiss, R. Tommasini, R. London, J. Park, M. Busquet, M. Klapisch, V. N. Shlyaptsev, and J. J. Rocca, "Energy penetration into arrays of aligned nanowires irradiated with relativistic intensities: scaling to terabar pressures," Sci. Adv. **3**, 3–11 (2017).